Using PMU Data to Increase Situational Awareness

Final Project Report

Power Systems Engineering Research Center

Empowering Minds to Engineer
the Future Electric Energy System

Using PMU Data to Increase Situational Awareness

Final Project Report

Project Team

Tom Overbye, Project Leader
Pete Sauer
University of Illinois at Urbana-Champaign

Chris DeMarco
Bernie Lesieutre
University of Wisconsin-Madison

Mani Venkatasubramanian
Washington State University

PSERC Publication 10-16

September 2010

Information about this project

For information about this project contact:

Thomas J. Overbye
Fox Family Professor of Electrical and Computer Engineering
University of Illinois at Urbana-Champaign
1406 W. Green St
Urbana, IL 61801
Tel: 217-333-4463
Fax: 217-333-1162
Email: Overbye@illinois.edu

Power Systems Engineering Research Center

The Power Systems Engineering Research Center (PSERC) is a multi-university Center conducting research on challenges facing the electric power industry and educating the next generation of power engineers. More information about PSERC can be found at the Center's website: http://www.PSERC.org.

For additional information, contact:

Power Systems Engineering Research Center
Arizona State University
577 Engineering Research Center
Tempe, Arizona 85287-5706
Phone: 480-965-1643
Fax: 480-965-0745

Notice Concerning Copyright Material

Acknowledgements

This is the final report for the Power Systems Engineering Research Center (PSERC) research project titled “Using PMU Data to Increase Situational Awareness.” We express our appreciation for the support provided by PSERC’s industrial members and by the National Science Foundation under grants NSF IIP-0968983, 0968833 and 0968818 received under the Industry / University Cooperative Research Center program.

The authors would also like to convey special acknowledgement to the PSERC IAB member companies who provided direct assistance with this project including BPA, Entergy, EPRI, Exelon, MISO, ISO New England, PowerWorld, PJM, Quanta, and TVA.

Executive Summary

With the large-scale deployment of PMUs in the U.S. and worldwide, a recurring theme has been the question of how to best extract useful "information" or "knowledge" from the very voluminous data that PMUs provide. While the direct control center display of PMU-based data is certainly important, particularly bus voltage angle values, this project focused on techniques the go beyond direct display of the raw PMU data. That is, the project focused on how information could be extracted from the PMU data, and then how this information could be used to improve power system situational awareness. Five different aspects of the problem are considered in Chapters 2 through 6.

Chapter 2 considers how much information could be gleaned from the PMU data with an approach that makes minimal use of other *a priori* information about the system status and model parameters. It is based on a data analysis tool that has been widely utilized for compression and feature extraction in other industries: the Singular Value Decomposition (SVD). The SVD method for PMU data processing views the physical power system as a power flow solver – taking time varying loads/injections as inputs, and producing PMU-measured angles and voltage magnitudes as outputs. By observing a time window of PMU measurements over an interval, forming a matrix of data, and computing the singular value decomposition of this matrix as this window "slides" forward in time, the Chapter 2 algorithm characterizes important aspects of the system's input-to-output behavior. When the system is highly stressed, one sees outputs vary much more dramatically in response to time variation of the inputs. This efficiently computes information closely related to the Power Flow Jacobian matrix conditioning, *with none of the state estimator and network data required to compute the PF Jacobian matrix itself – the algorithm uses PMU measurements only*. Conditioning of the Power Flow Jacobian is a general indicator of robustness of a system operating point; more specifically, the smallest singular value of the power flow Jacobian (i.e., as it approaches zero) has long been utilized as a first indicator of vulnerability of a system to voltage collapse. Hence, one of the outputs of SVD-based PMU processing algorithm serves as a real-time indicator of system stress, tracking a well-established voltage stability performance metric without the need for detailed network parameter values or state estimator results.

Chapter 3 presents an algorithm on how PMU data can be used to enhance existing power flow algorithms to improve situational awareness. The motivation for this application arises because in a variety of situations SE results may not be available. For example, smaller utility control systems may not have an SE, the SE may have failed to converge during rapidly changing system conditions, there may be a need to combine SE results with a larger system model, or people involved in nonoperational aspects of the power grid, such as marketers and power system planners, may not have access to SE results. But often a power flow case is available that at least approximates (to some degree) the current operating condition. The Chapter 3 algorithm shows how existing linear programming (LP) based optimal power flow algorithms (OPF) can be used to change a power flow operating point to better match the bus voltage angles coming from the PMUs. The algorithm is demonstrated using a three bus case and a 13,000 bus case.

Chapter 4 presents the visualization of PMU-derived information associated with power system electromechanical oscillations using the Washington State University Oscillation Monitoring System (OMS). The inputs to the OMS are selected PMU bus voltage measurements. When a disturbance is detected the OMS uses a real-time Prony analysis with a moving time-window to determine the oscillation frequency and damping ratio. Results are visualized with a user-friendly, web-page interface.

Two example visualizations are presented. In the first, the Damping Monitor display, there are three major areas. Left top is a frequency vs. damping ratio point chart, which shows all the modes in the frequency domain, and their damping ration on y-axis. The right top corner shows the time and a brief summary, which includes the status of each mode. The bottom of the display is the mode shape area, which shows mode shapes of up to 4 modes, in a radial fashion. In the second, the Event Monitor display, there are two areas. The top area shows the mode frequency and the damping ratio with a dial like chart. The bottom part shows the mode shape, as in the Damping Monitor display.

Chapter 5 considers how PMU data can improve situational awareness by improving the load models used for power system analysis platforms. The mathematical models for loads used in most security (operational reliability) analysis range in detail from simple impedances to generic dynamic models and full-blown induction motor models. These load models typically have various parameters that describe their behavior and power consumption. In hour and day-ahead analysis, the loads are essentially based on power forecasts. Two things about these load models are important in the analysis. The first thing is the model structure (static, dynamic etc.); the second is the model parameter values.

Since PMUs provide virtually real-time values of voltages and currents, they have the potential to be useful in producing virtually real-time load models for security (operational reliability) analysis. If the PMU data come from locations that could be considered “load buses”, then analysis of these measurements could provide information on the structure of the load model and the parameters of the model. This portion of the project developed a process to perform this analysis.

This process was then evaluated with simulated phasor data using a 3-machine, 9-bus system, and a 9-machine, 30-bus system. For each system, several cases with different load models were simulated using the automatic identification procedure. The voltage variation was detected to start the estimation process. The load type was determined by inspecting the P-V relation and by using the self-augmented model. LMA was used to estimate model parameters. Finally, the estimation results were validated by using the data after that until another voltage variation was detected. The results from both test cases using simulated phasor data indicate that the method could become a valuable tool for model identification in real time.

The application of PMU data to improve reactive power monitoring and control is considered in Chapter 6. The ability to supply reactive power when it is needed can help a system to obtain a new stable operating point instead of becoming unstable. Generally, such reactive power control occurs only at the transmission system level. Chapter 6 develops a framework to allow control of distributed reactive-power capable devices located near the end-user. In particular, inverters such as those connected to PV

panels and pluggable-hybrid electric vehicles (PHEVs) can be used to operate at a leading power factor and thus supply reactive power.

The communication and control for these reactive power resources can be coordinated in a hierarchical way. First, the voltage problem must be detected. Then, the appropriate response action needed to correct the voltage problem is computed. The solution at this stage gives locations and amounts of reactive power needed to correct the problem. Action requests are formulated and sent to an agent, which may be located in a relay on a feeder. This feeder agent may be upstream of several other relays and load controllers. The requests propagate downward. At each level, a set of response actions needed to fulfill the request are determined and sent to the next level in the hierarchy. Results are demonstrated using the IEEE 24-bus reliability test system.

Future Research Steps

With the rapid growth in PMU installations across many power systems it is clear that PMUs will play a role of increasing importance in power system operations. While this project has presented solid research for moving forward, there is certainly more work to be done. The SVD work from Chapter 2 needs to be further tested and validated; also applications to other PMU-based measurements should be considered. While the Chapter 3 work of incorporating PMU-measurements into the power flow could also benefit from additional testing, it is at the stage in which commercial implementation should be considered. The Chapter 4 OMS is currently undergoing utility testing; the associated visualizations could be enhanced based upon the results of this testing. The Chapter 5 load modeling work should having additional testing with actual PMU data; it could also be extended to consider more dynamic load models, such as induction machines and other devices such as synchronous generators. Last, the Chapter 6 use of PMUs for improved reactive power modeling as advanced to the point in which actual prototype installations can be considered.

Table of Contents

List of Figures

List of Tables

1. Introduction

1.1 Background and Problem Overview

According to the August 2003 blackout report [37], one critical need for the power industry is an increase in its situational awareness. Over the last two decades much work has been done in determining the best ways to represent traditional SCADA and EMS information to operators to increase their understanding of grid conditions, with much of this work now finding its way into electric utility application. As this work has progressed, new devices have continuously been added to the power grid. One of the most interesting new devices deployed on the power system, the phasor measurement unit (PMU) [1], is just now beginning to see wide scale deployment in electric utility control center supervisory applications.

From a situational awareness perspective there are three issues that make PMU measurements unique. First, they can provide relatively high measurement rates, with values of 30 times per second typical. This allows them to capture previously difficult to observe power system dynamics. Second, they provide a direct measure of the voltage and current phase angles, permitting these values to be displayed without the need to first perform a state estimation. This, coupled with their high measurement rate, means that voltage angles can now be used directly in power system visualizations. Of course from the voltage and current phasors other quantities such as real and reactive power flow can be easily calculated. Third, they can quickly provide synchronized values from anywhere within an entire interconnect. This allows their direct usage in interconnect-wide visualizations.

To-date, most of the research regarding PMU integration into control centers has focused on applications in state estimation [2] and, more germane to this effort, on direct visualization of the bus voltage angles. For visualization the techniques that have been presented in the literature include a) the use of phase angle contouring, b) the geographic placement of bus voltage angle pie charts, and c) a combined dial like display that shows the voltage angles from a number of buses simultaneously. As examples, Figure 1.1, which reproduces Figure 5 of [3], shows a nice example of color contouring applied to the WECC system; Figure 1.2, which reproduces Figure 4 of [3], shows how pie charts placed in a geographic context can be used to display voltage phase angle variation across the WECC; Figure 1.3 which reproduces slide 10 of [4], shows a single representation of approximately thirty bus voltage phase angles.

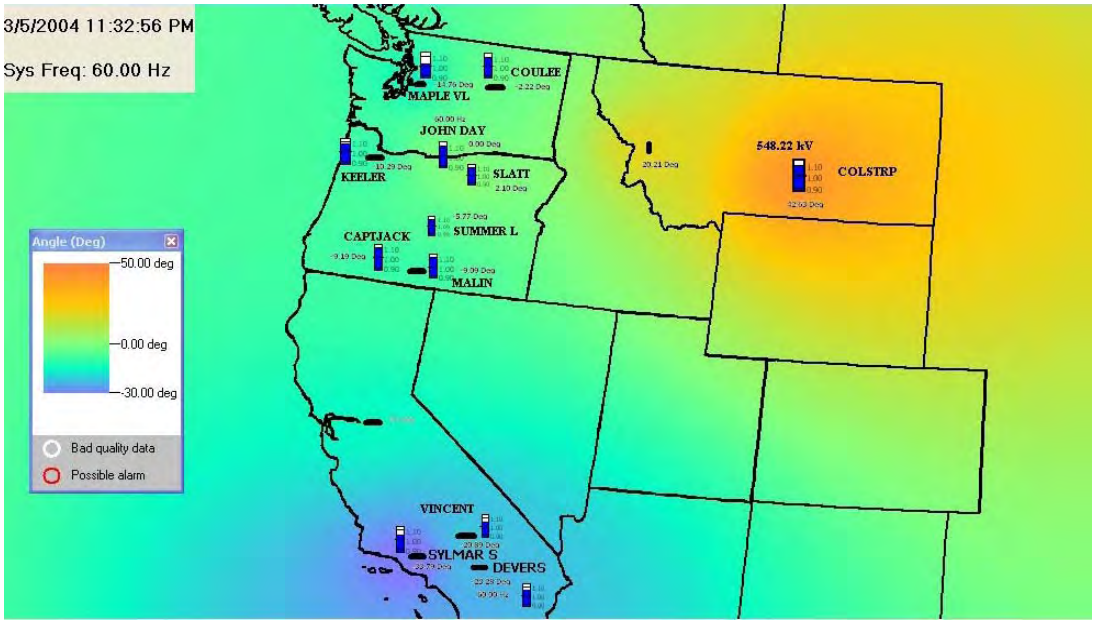

Figure 1.1 WECC Display of voltage phase angles as a color contour and voltage magnitudes using thermometers

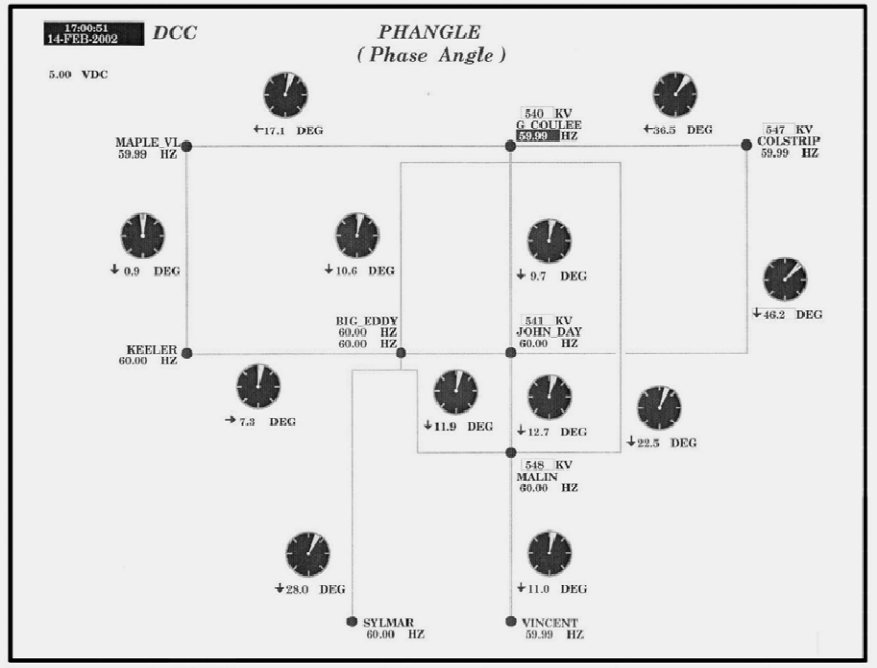

Figure 1.2 BPA bus phase angle display from 2004

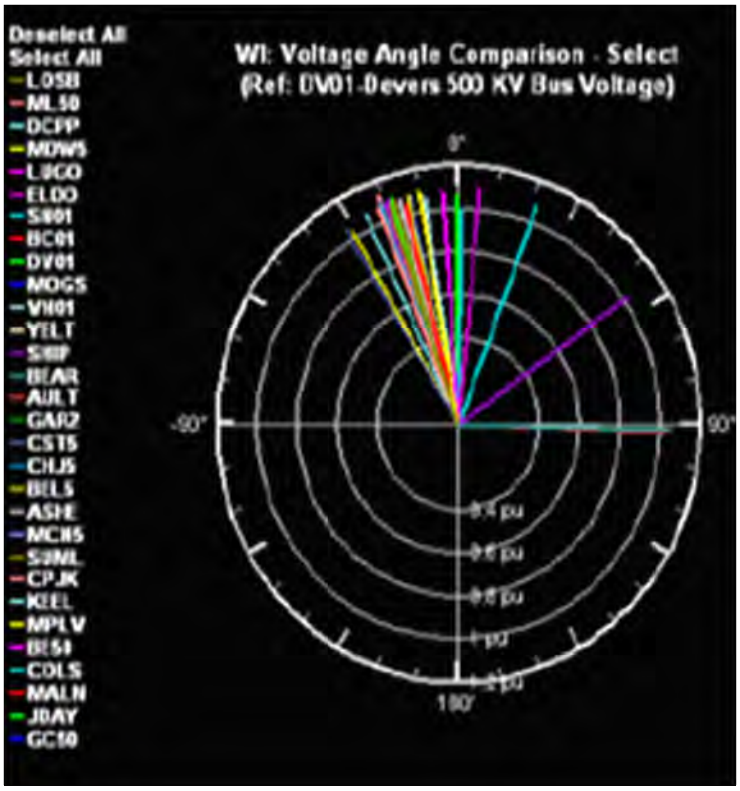

Figure 1.3 Bus voltage phase angle comparison dial

For this project, rather than just seeking to expand on the earlier work done in direct visualization of the bus voltage angle values, we took a broader approach looking at how information contained within the PMU values (with a focus on bus voltage magnitudes) could be extracted to help in the broader situational awareness problem.

1.2 Report Organization

This report is organized into seven chapters. Chapter 2 presents a technique to use PMU-based information to determine a system voltage stability metric that makes minimal use of other *a priori* information about the system status and model parameters. Chapter 3, discusses how PMU information can be used within existing power flow algorithms to enhance system situational awareness in situations in which a full state estimator solution is not available. Chapter 4 presents some visualization techniques that can enhance real-time monitoring of power system oscillations using PMU values. Chapter 5 looks into how PMU values can be used to improve the load models used in the power flow and transient stability applications. Chapter 6 considers how the improved system observability offered by PMUs can be coupled with the growth in distributed reactive power resources to improve the overall grid voltage support. Finally, Chapter 7 provides a summary and directions for future research.

2. A Singular Value Decomposition Approach to PMU Data

2.1 Background

The Synchronized "Phasor Measurement Unit" (PMU) is familiar to most power engineers. Briefly, a PMU measures a windowed Fourier transform ("phasor") of the nominally sinusoidal voltages, currents, powers throughout grid. The innovation of the last two decades has been to use Global Positioning Satellite (GPS) technology to facilitate precise, low-cost time synchronization of these signals across large geographic distances. The result has been a growing number of synchronized measurements, typically at 30 or 60 Hz reporting rates (with analogous rates for 50 Hz systems), across a continental scale.

With the large-scale deployment of PMUs in the U.S. and worldwide, a recurring theme has been the question of how to best extract useful "information" or "knowledge" from this very voluminous data that PMUs provide. The portion of the project reported here sought to address precisely this need, in a fashion that made minimal use of other *a priori* information about the system status or model parameters. In proposing this work, the techniques sought were described as a "model-free" evaluation of the power systems' operational condition, to stress that the methods sought would almost exclusively use the real-time measurement data of the PMU's themselves. In slightly more precise terms, the question to be addressed is: "how does one compress PMU data, and use it to compute real-time performance metrics that can inform grid control action?"

The need for data reduction, compression, and feature extraction from voluminous data sets is hardly unique to power industry. Geological data processing, gene sequencing, bio-informatics, electronic commerce customer classification – all of these are problems with similar characteristics. There exists a long history of methods to achieve data set reduction/compression and feature identification in huge data sets. In both data compression and feature extraction, a common "Swiss Army Knife" for treating large data sets in many fields has been that of the Singular Value Decomposition (SVD) [5].

In compression applications, SVD-based methods were an early competitor to the now ubiquitous jpeg algorithms for compression of digital image data. As will be reviewed in more detail below, the SVD is fundamentally a factorization of a matrix, that explicitly identifies and rank-orders the matrix's "gains" (its singular values), while also identifying each "direction" (singular vectors) along which these gains act. From this perspective, its use as a image data reduction tool is apparent: one computes the SVD factorization for the two-dimensional array (matrix) representing an image, and compresses it by throwing away information associated with those directions having very low gain.

For feature identification (in loose terms, the extraction of "knowledge"), one of the most common applications of SVD for large time and spatial series data sets is that of Principal Component Analysis (PCA) [6]. In its simplest form, the premise of PCA is that time sequence of vectors of data may be approximated as arising from Gaussian processes. In this context, the goal of PCA, using the singular value decomposition, is to identify coordinate bases that decompose the components of the observed vectors into uncorrelated variables – the "principal components." In this context, the singular values identify the variance of each of the uncorrelated Gaussian random variables, while the

singular vectors identify the change of coordinates between the original measurement data and the new, uncorrelated coordinate system.

These types of applications of SVD have precedent in prior PSERC-supported work. SVD methods were used as a filtering method for noise reduction in PMU data, as a step for estimating oscillatory modes in grid electro-mechanical dynamics (PSERC project S-29, led by M. Venkatasubramanian). Principal component analysis and its nonlinear variants were employed for demand prediction in LMP market risk management (PSERC project M-17, led by S. Deng).

The use of SVD methods to be proposed here, while building on concepts of Principal Component Analysis, and on the prior PSERC work, has a decidedly different flavor. Our underlying premise views the physical power system as defining a relation between its inputs (primarily loads at each bus, varying in time), mapped through the power flow behavior of the network (influenced by line switching and other contingencies), producing the PMU measured outputs of bus voltage magnitudes and phase angles. While this perspective is intentionally oversimplified for descriptive purposes here (i.e., PMU measurements may certainly include some of the "inputs," as well as flow quantities), it provides a means to think about what information may be extracted from PMU data. In essence, we view the physical power system as power flow solver – it takes time varying load as input, and maps it to the PMU-measured angles and voltage magnitudes as outputs.

By observing a time window of PMU measurements over an interval (thereby forming a matrix of data), and watching the behavior as this window "slides" forward in time, we should be able to observe characteristics of the map from inputs to outputs. When the system is highly stressed, we expect to see outputs vary more dramatically in response to time variation of the inputs. In terms of the SVD algorithms we propose, we should see the largest singular value (the maximum "gain" of the map) grow in size as the system becomes stressed. As we will elaborate when describing the proposed algorithms in more detail below, our hypothesis is that we can capture information closely related to the Power Flow Jacobian matrix conditioning, *by computations using PMU measurements only*. Conditioning of the Power Flow Jacobian is a general indicator of robustness of a system operating point; more specifically, the smallest singular value of the power flow Jacobian (i.e., if it approaches zero) has long been advocated as a first indicator of vulnerability of a system to voltage collapse [7]. To use these insights, we will make assumptions about the structure of the power flow problem, but will not assume any knowledge of the parameters that "feed" the power flow (i.e., no system topology or line admittance information will be used). This measurement-only framework delivers on the "model free" goal of the original project proposal.

The new contribution to be reported here can be summarized in the following:

Claim: A windowed SVD computation on PMU data tracks a well-established voltage stability performance metric, whose computation traditionally would normally require state estimation of operating point, and full information on network and load models. The method here instead offers a "model free," real-time indicator of quasi-steady state grid performance, particularly relevant for control schemes to guard against voltage instability.

2.2 Singular Value Decomposition (SVD) Overview

The SVD has become a very widely adopted tool in matrix analysis for a huge variety of applications; for a highly accessible article outlining its many applications, readers are encouraged to consult [5]. As noted above, in simplest algebraic terms, the SVD is simply a factorization of a matrix. Anticipating our application to the power flow formulated in real-valued coordinates of voltage phase angles and magnitudes, we consider ***J*** as an *lxn* matrix of real-valued elements, rank m, decomposed as

$$J = U \begin{bmatrix} diag(\sigma_1, \sigma_2, ..., \sigma_m) & \mathbf{0} \\ \mathbf{0} & \mathbf{0} \end{bmatrix} V^T \tag{2.1}$$

where ***U*** and ***V*** are unitary matrices (i.e., $\boldsymbol{U}\boldsymbol{U}^T$ = Identity Matrix), the boldface **0** entries represent all zero entry matrices of appropriate dimension, and σ's positive, real-valued scalars. From this algebraic perspective, the unitary matrix $\boldsymbol{V}^T$ represents a change of coordinates on the domain of the matrix (the "input" space of *n*-dimensional vectors). In this new coordinate system, the matrix operation may be viewed simply as scalar, positive, real "gains" $\sigma_1, \sigma_2, \ldots, \sigma_m$ acting along *m* basis component directions, with zero gain along the remaining *n-m* basis directions. The unitary matrix ***U*** then changes coordinate back to the native coordinate system for the range of ***J*** (the "output" space of *l*- dimensional vectors).

A commonly used illustration in textbook approaches to the SVD is to look at these operations geometrically, and this geometric perspective is particularly useful in understanding our use of the SVD here. Suppose one had a set of unit length (2-norm) vectors in the input space, constituting all possible points on the surface of the Euclidean unit ball. If each of these vectors is operated on by the matrix ***J***, the result in the output space is a generalized ellipse. The major axis of the ellipse aligns with the vector formed by the first column of ***U***, and has length σ_1. The smallest non-zero axis of the ellipse aligns with column *m* of ***U***, and has length σ_m. For the case of matrix ***J*** being row rank deficient, the remaining *l-m* columns of ***U*** define directions along which the ellipse has zero expanse. This operator gain geometric viewpoint on the SVD is pictured below.

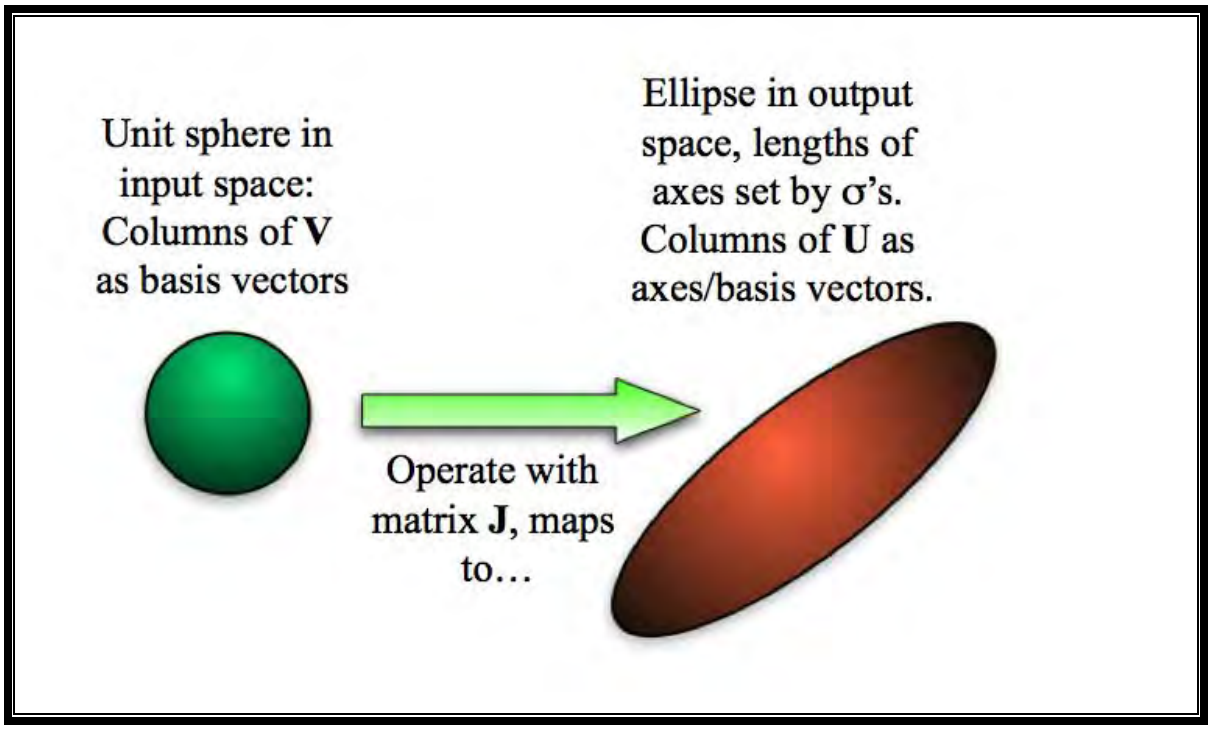

Figure 2.1 Geometric illustration of SVD of matrix ***J***

2.3 Singular Value Decomposition in Data Compression

As noted above, there has been a long-standing history of use of SVD in data handling. The basic idea is quite simple: consider sequential acquisition (1, 2, …*k*…) of a vector of "*l*" measurements, denoting each such *l*-dimensional vector as $\underline{m}[k]$. For running window of length *n*, construct a matrix, denoted $\boldsymbol{M}[k]$ as

$$\boldsymbol{M}[k] := [\underline{m}[k-n+1], \underline{m}[k-n+2], \ldots \underline{m}[k]\ ]$$

Observe that at each new acquisition time *k*, $\boldsymbol{M}[k]$ is updated by adding the new column on the right, $\underline{m}[k]$, and discarding the "oldest" data vector $\underline{m}[k-n]$, maintaining *n* columns. For our application, we may consider an vector of PMU measurements at time sample instant *k*, organized as a column, comprising $\underline{m}[k]$. A *n*-length window of such vectors then composes matrix $\boldsymbol{M}[k]$. In this context, consider a simple extreme case in which $\boldsymbol{M}[k]$ contains minimal information, and how this is reflected in the SVD. In particular, suppose the matrix $\boldsymbol{M}[k]$ consisted of the unchanging measurement values repeated in every column, indicating that the PMU measurements were unchanging over the time window. In this case, $\boldsymbol{M}[k]$ would, by definition, have rank of 1, and hence only one non-zero singular value. The entire matrix could be exactly reconstructed as

$$\boldsymbol{M}[k] = \sigma_1 \mathrm{x}[\textit{column 1 of } \boldsymbol{U}]\mathrm{x}[\textit{row1 of } \boldsymbol{V}^T]$$

i.e., instead of *l*x*n* components of real valued data, the redundancy in this case is such that we need only one scalar, one *l*-dimensional vector, and one *n*-dimensional vector to represent $\boldsymbol{M}[k]$.

2.4 Interpreting PMU Data in the SVD Perspective

Consider a simple, quasi-steady-state, input-output view of the operation of the power system: the primary inputs are the continuously varying P-Q injections (loads being negative injections); the primary outputs are δ's and V's of PMU data. As noted previously, the mapping between them is influenced by network switching, component failure, other structural changes in the transmission network and switched shunt devices. Driving the time variation of this process, we assume that injections have both a slowly varying component (e.g., the 24-hour load curve), and smaller magnitude, much faster random variation arising from the aggregation of many hundreds of thousands of individual pieces of customer equipment switching on and off in the loads connected to a particular substation. Both central limit theorem arguments and historic measurement data studies [7] suggest that the random part is often reasonably approximated as zero mean, small variance filtered white noise (as a rough estimate, one might take the variance to be approximately ~ 1% nominal load magnitude).

Using this perspective with our previous suggestion of assembling a window of PMU measurements into a matrix $\boldsymbol{M}[k]$, let us suppose that the window length is short relative to the longer time scale on which slow, large magnitude load variations typically occur (i.e., if the slow load variation is the 24 hour day, the window length would be held to a duration less, typically much less, than 5 minutes). Under these circumstances, the variation in inputs (injections/loads) over the window is primarily driven by the random variation described above. While oversimplifying for conceptual purposes, suppose these random load variations at each bus were all of uniform magnitude, with this variance scaled to a normalized value of 1. In this case, our geometric picture would be very much like that of the figure above, mapping a unit ball in the input space, to a generalized ellipse in the output space. The inputs would be samplings vectors of injection variations, with each sample being a vector on a unit ball. This unit ball would be centered on the nominal injection values associated with the slow variation, approximated as constant over the short time window comprising $\boldsymbol{M}[k]$). The mapping from inputs (load variations away from nominal values) to outputs (variations in phasor angles and magnitudes) would be that determined by the incremental behavior of the power flow solution; i.e., the mapping $\boldsymbol{J}$ would approximately correspond to the **inverse** of the power flow Jacobian about the nominal operating point over the window of interest. This conceptual picture is represented in the figure below.

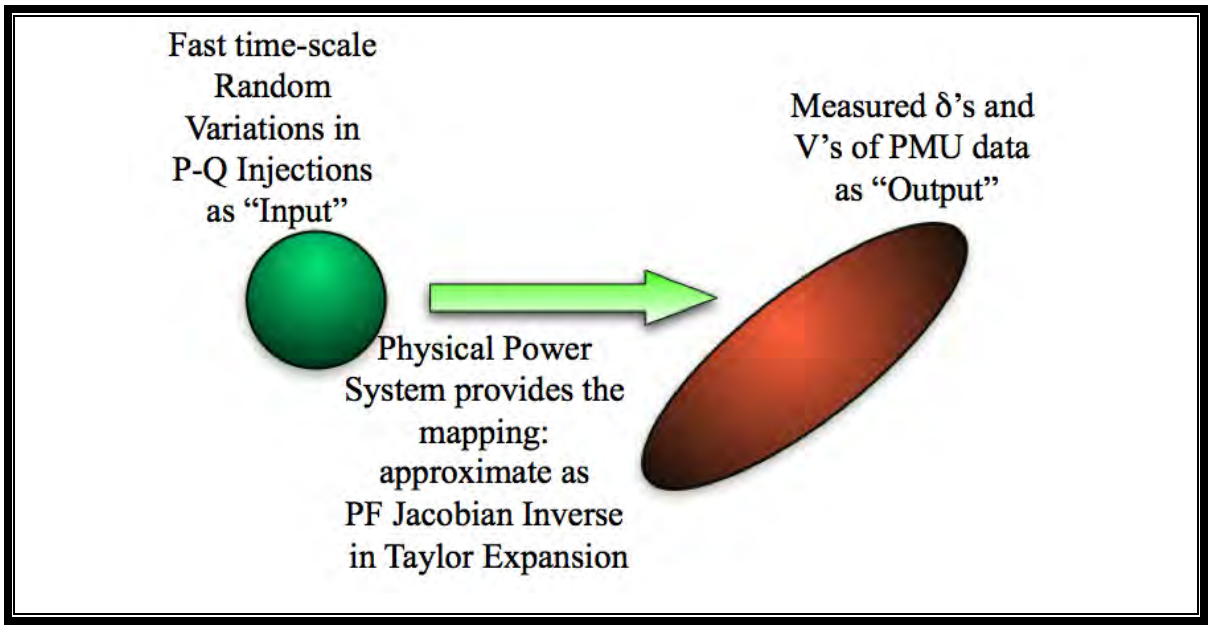

Figure 2.2 Geometric view of the incremental approximation to power flow mapping

As suggested in the figure above, it is important to grasp the geometric interpretation of the data captured in the matrix of windowed PMU data $\boldsymbol{M}[k]$: it is a sampling of n vectors of PMU measurements, each of which is a point on the surface of the "output ellipse" in the figure. Provided the random variation of the injections is sufficiently "rich" over the time window sampled (i.e., the variations move across many directions in the input space), we can expect to get a wide sampling of points across the surface of the output ellipse. In this way, one captures information about the characteristics of the inverse power flow Jacobian that maps from the inputs to outputs. In particular, if the inverse power flow Jacobian has a maximum singular value of very large magnitude (correspondingly, if the smallest singular value of the Jacobian itself is approaching zero, as per [7]), then this is reflected in very high sensitivity from injection variation to phase angle and voltage magnitude variation.

This is the type of ill conditioning of operating point that we seek to quantify in computing the SVD measure for the windowed PMU data. In particular, we propose to track the largest singular value of a running window of PMU measurements; in the notation developed, we propose tracking the time varying quantity $\sigma_1(\boldsymbol{M}[k])$. In addition, the components of corresponding singular vector $\boldsymbol{U}_1$ carries the very useful information of the relative contribution of each measurement to this largest singular value. While one could certainly consider additional information to be garnered from singular values and vectors other than the largest, these refinements were not pursued in the course of research presented here, and await future work.

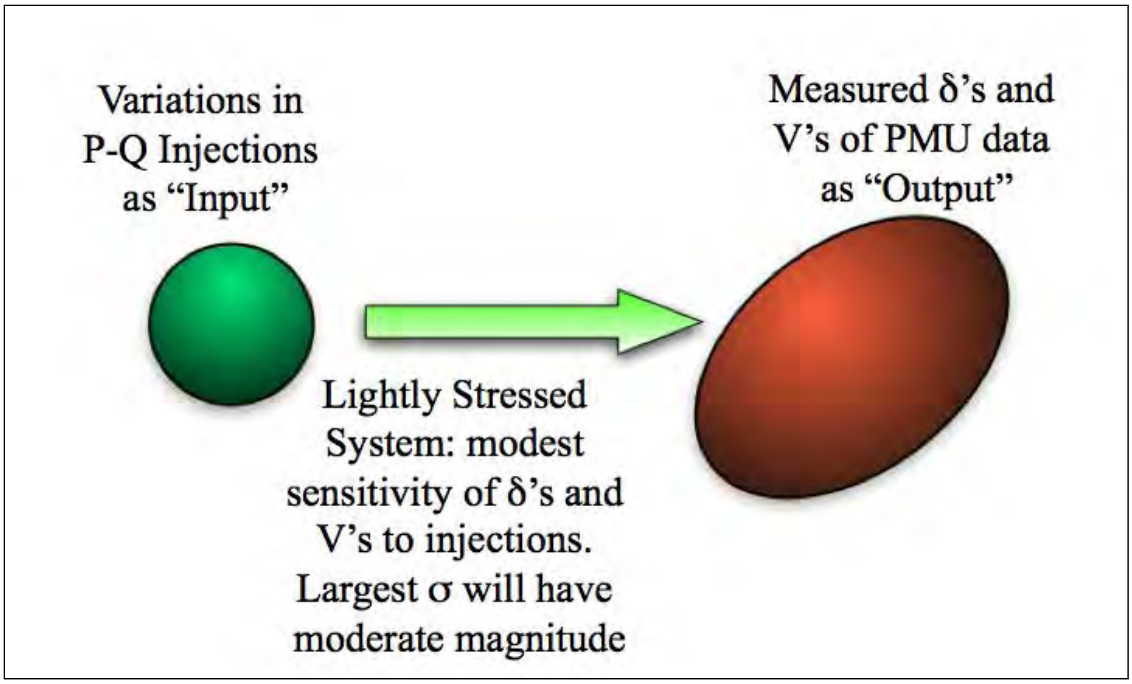

Figure 2.3 Geometric view of power flow mapping – lightly stressed case

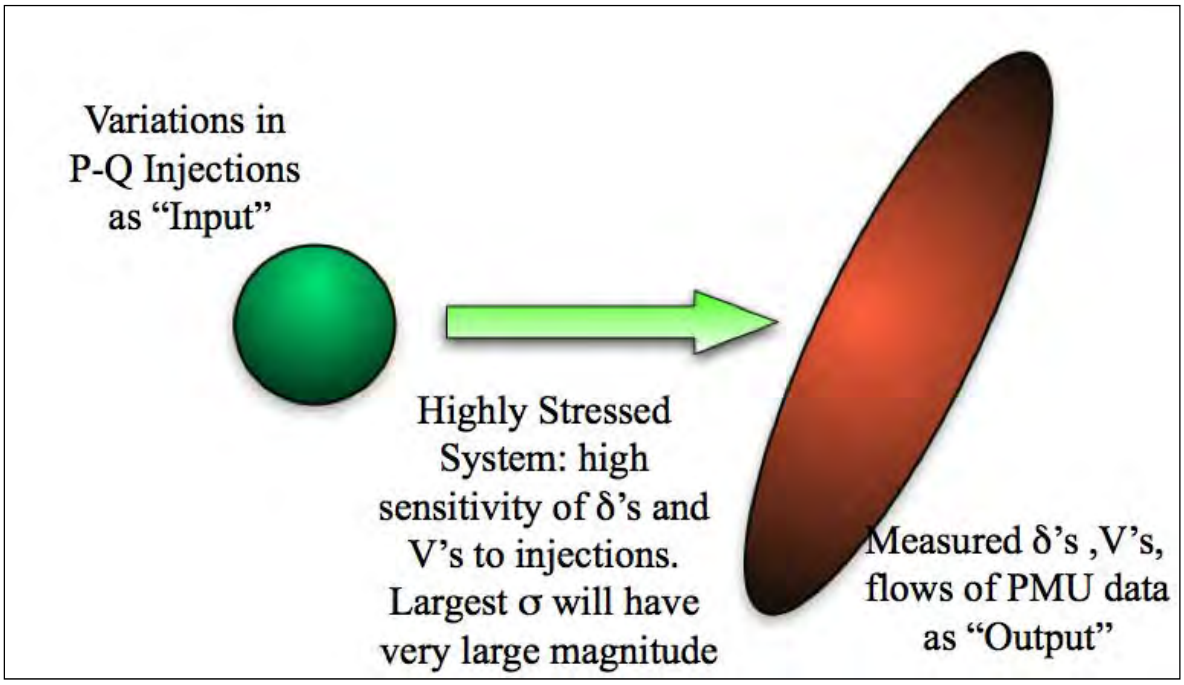

Figure 2.4 Geometric view of power flow mapping – highly stressed case

2.5 Caveats and Practical Issues

In considering the conceptual picture described in the preceding section, there are several practical issues and departures from the ideal to be considered. Most obviously, while it is clear that PMU deployment rapidly expanding in the U.S. and around the globe, one may still only expect only a modest subset of all phasor angles and voltages to be available as PMU measurements (i.e., PMU's measurement density is a modest % of all bulk power system buses). Therefore, in terms of the viewpoint of the preceding section, the mapping that produces the available PMU measurements is only a **subset of the rows** of the Power Flow Jacobian Inverse. A key criterion for using the method proposed here is that the largest singular value of this smaller matrix produce behavior comparable to that of the full Jacobian inverse.

While this topic remains in need of more rigorous analytic study in future work, heuristic study (i.e., sample comparisons in a large number of numeric test cases) conducted here indicated that a density of PMU measurements at approximately 10% of all buses, when this buses were distributed throughout the network, typically produced very similar behavior of largest singular value of the reduced Jacobian inverse (with rows corresponding just to measurement locations) and that of the full Jacobian inverse (all rows). This framework may offer a very tractable formulation for optimizing measurement placement, and in future work it will prove interesting to compare this metric for quality of measurement placement with more established work that characterizes measurement placement quality based on observability and conditioning of the state estimation problem.

Another aspect of the scenario above that bears scrutiny is the assumption that the output quantity of interest is the deviation of PMU measurements away from a nominal value for the window period. As a pragmatic computational heuristic to capture the "nominal," it is natural to simply compute the running mean of the each PMU measurement over the window. If this mean is subtracted from the actual measurement, and the $\boldsymbol{M}[k]$ is constructed from these deviations, the algorithm becomes very close to the computation that would be performed in PCA.

Our numerical experience to date in both synthetic test systems and with actual PMU data suggests that this form of the algorithm is useful for identifying points in time at which switching event of contingencies occur, but less useful as a measure of overall conditioning and "stress level" on the system. Our experience suggests that maintaining the "raw" PMU measurements in constructing $\boldsymbol{M}[k]$, without any subtraction of the mean, provides the best metric of system stress. We argue that by this approach, one is capturing both the effect of major changes in operating point that may stress the system, along with changes in the conditioning of the power flow Jacobian. However, we must also again stress that the work presented here is only a preliminary scoping study into the possibilities of this newly developed method for using PMU data. Undoubtedly, future work will reveal improved algorithms for using both the raw, instantaneous singular value behavior, and the evolution of the means of the PMU measurements.

2.6 Computational Experiments in Synthetically Generated Data

The initial proof-of-concept studies made use of the IEEE 14 and 118 bus test systems, with both power flow and singular value decomposition computations performed in the MATLAB environment. The basic procedure in these studies was straightforward, and may be described as follows:

- Construct sequential power flow computation;
- "Drive" computation by time sampled loads & generation dispatch, along 24 demand curve, with 1% random load variation superimposed (computation to follow uses 15 sec sampling interval, 5760 samples per 24 hours);
- "Stress" system by randomly chosen switching in and out of lines over 24 study period;
- For (subset of buses) record angles and voltage magnitudes as hypothetical PMU measurements;

In each of the test system study scenarios, the key premise is that the largest singular value of the rows of the inverse power flow Jacobian provided a benchmark of system conditioning. We will examine the impact of density of measurements by beginning from a case for the IEEE 14 bus test system in which every row of the inverse Jacobian is used, corresponding to the idealized case of a PMU measurement for every bus angle and magnitude. This will be followed by test case for the IEEE 118 bus system in which a bus measurement density of less that 10% is used (11 buses assumed instrumented, out of the possible 118). Two different selections of the 11 buses for measurements will be illustrated.

Note that benchmark information from the power flow Jacobian is *not* expected to be available in real-world application of the SVD measure to PMU data, but rather serves as an off line test of the quality of the "model-free" computation, using the pseudo-PMU measurements only. In particular, we'll seek to characterize the quality of the SVD-based PMU measure by comparing plots of:

- Largest singular value of windowed PMU measurement matrix (labeled as "Sub-window SingVal" in plots to follow);
- Largest singular value of computed from appropriate rows of power flow Jacobian inverse (labeled as "SingVal inv-Jacobian" in plots to follow)

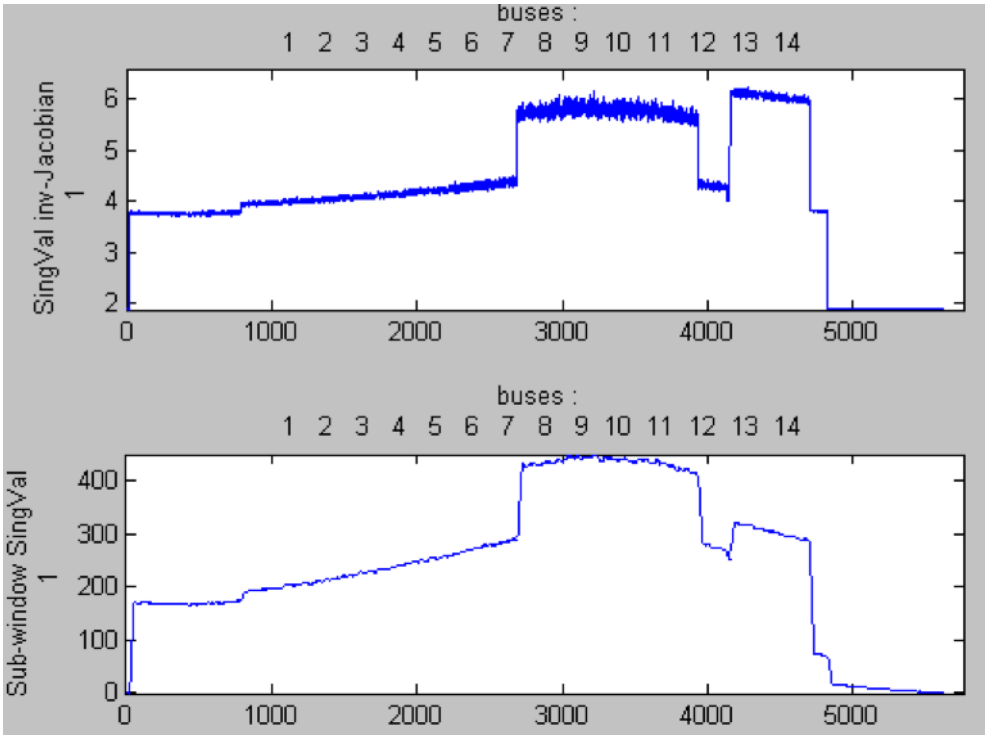

Figure 2.5 IEEE 14 bus example – idealized limit of PMU at every bus

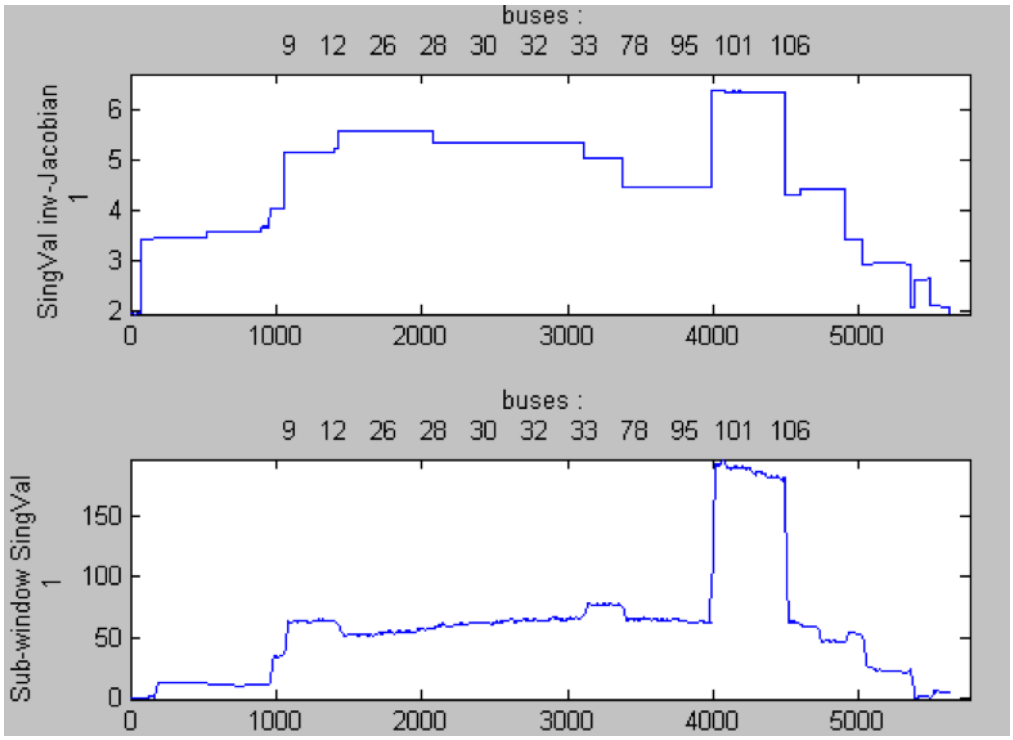

Figure 2.6 Figure: IEEE 118 bus case A – PMU penetration 11 out of 118 buses (PMU placement for case A: buses 9,12, 26, 28, 30, 32, 33, 78, 95, 101, 106)

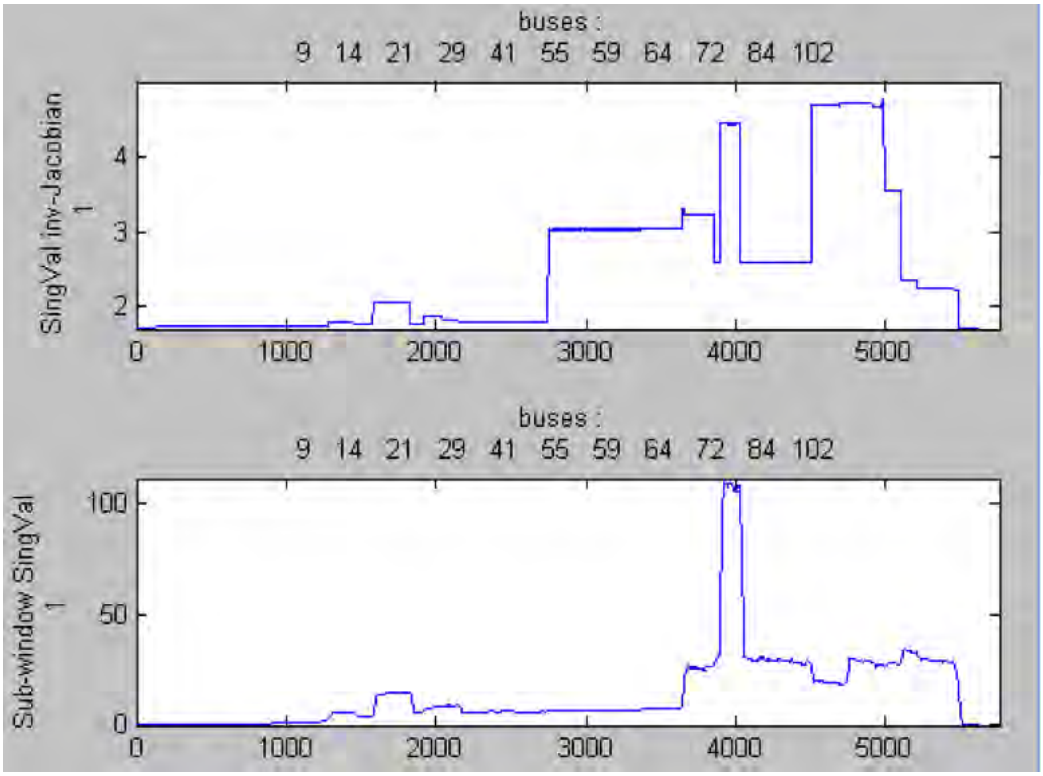

Figure 2.7 IEEE 118 bus case B – PMU penetration 11 out of 118 buses (PMU placement case B: buses 9,14, 21, 29, 41, 55, 59, 64, 72, 84, 102)

Interpreting these graphic results, we note first the very close match in behavior observed for the maximum singular values for the two measures in the 14 bus system test, for the idealized case of all rows of the Jacobian inverse maintained (i.e., every bus voltage and phase angle available in the PMU measurement set). While the scaling of the SVD quantities is of course very different, the qualitative shape of the curves matches extremely well. Our anticipated applications would involving use of the full information (the Jacobian inverse) from off-line studies to identify the scaling factor between the SVD of the Jacobian inverse, and that of the PMU-based computation, as well characterizing a threshold level at which the system would be flagged as entering an emergency state. This threshold might vary, depending on which areas of the system were most affected (as would be indicated by information in the singular vector corresponding to the largest singular value, column 1 of $\boldsymbol{U}$).

The results for the 118 bus system, with measurement density of less than 10% of buses, indicates some degradation of the agreement between the more exact Jacobian inverse calculation, and that obtained from the pseudo PMU data. However, the degree of qualitative agreement between the two computations remains quite good. It would appear that with the reduced measurement density, there are some line switching event that stress the system (as indicated in the exact PF Jacobian inverse), and yet do not produce a large increase in the maximum singular value of the measurements. Roughly speaking, these system stresses are not observable from the measurement set employed. This reflects the

inability of a relatively small bus measurement set to fully capture the impact of all possible line outages.

2.7 SVD Tests on Bonneville Power Historic PMU Data Sets

Staff at BPA, under the direction of Mr. Dmitry Kosterev, have collaborated with faculty at the University of Wisconsin-Madison in evaluating and testing the SVD-based PMU measure. As part of this effort, several sets of representative historic PMU data were provided for testing within the SVD framework. While adherence to non-disclosure agreements and Critical Energy Infrastructure Information protections prevent extensive descriptions of the data sets and the areas and operating conditions they represent, these sets provided a realistic framework in which to illustrate the nature of the SVD-based computation and its resulting output. The faculty of the University of Wisconsin express their gratitude to Bonneville Power Administration for this cooperation and data sharing.

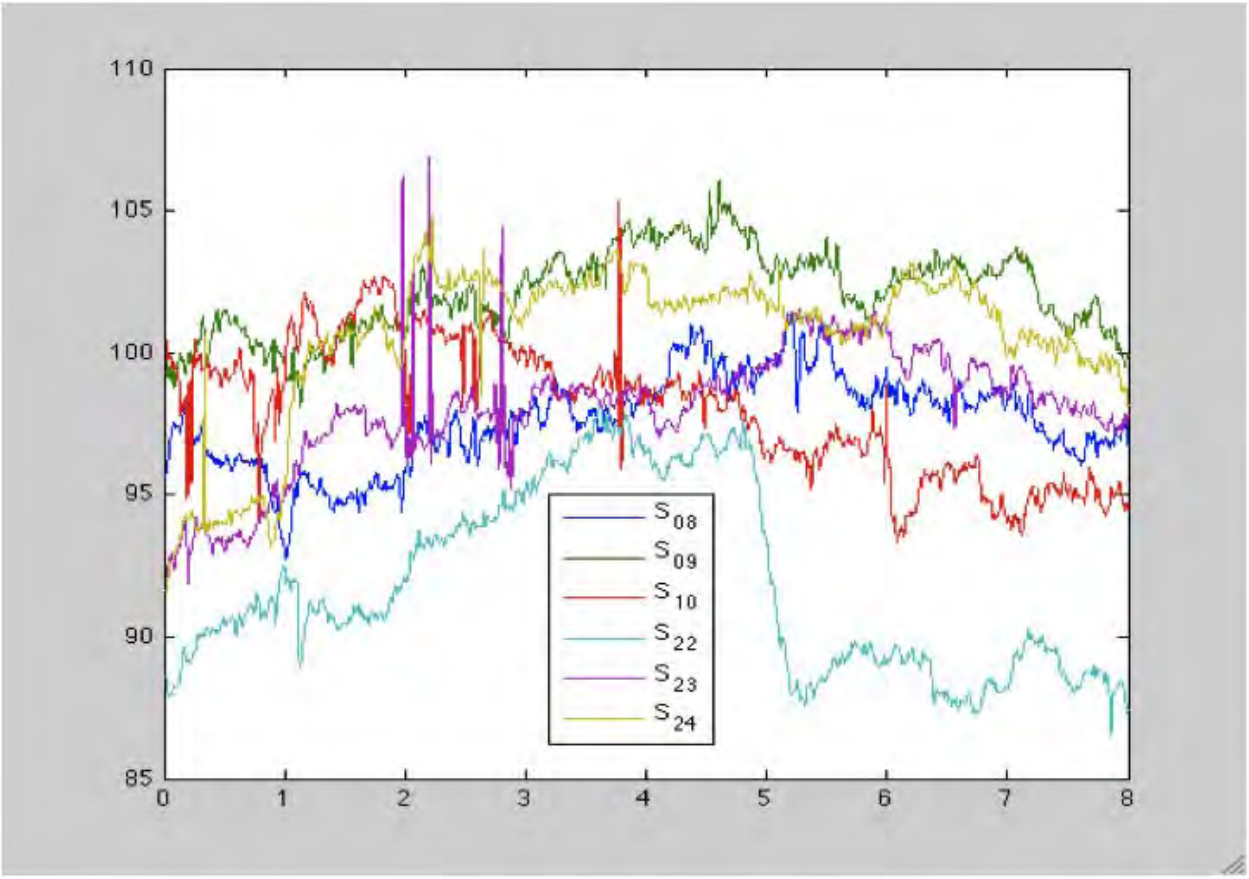

Figure 2.8 SVD-based PMU measure for BPA test data, 8-hour periods for 6 days, coded as S08, S09, S10, S22, S23, S24; horizontal axis hours, vertical axis maximum SVD on windowed measurements

The plot of results on the BPA data illustrate the largest singular value computed for a windowed measurement set of 52 PMU channels, at a reporting rate of 30 samples per second. Six different days of data were provided, identified by legends of S08, S09, S10,

S22, S23, and S24. Each data set included the same 52 PMU measurements, spanning an eight hour interval of time from 11:00 AM to 7:00 PM on each of the days studied. The plot is displayed with units of hours on the horizontal axis, with "zero-hour" corresponding to the start time of 11:00 AM. The vertical axis displays the numeric value of the maximum singular value computed from the matrix of windowed measurements. The algorithm as developed suggests a window length of two to three times the dimension of the measurement set; for the 52 measurements here, a window length of 150 was selected (specifically, the $\boldsymbol{M}[k]$ matrix was of dimension 52 rows, 150 columns). This window length of 150 samples, at a reporting rate of 30 samples/sec, corresponded to a 5 second window time interval. Hence the assumption of nominal injections remaining approximately constant over the window seems very credible. These computations did not have the benefit of an off-line, full information calculation of power flow Jacobian inverse against which to benchmark. Hence, the magnitude of the maximum singular value displayed on the vertical axis is meaningful only as a relative measure, to compare the degree of stress on the system across the six different days, at the different hours studied. However, even in this limited, relative interpretation of the SVD- measure, the BPA staff reviewing the results was that the SVD measure reported that these values agreed well with their engineering judgment as to the degree of system stress.

2.8 Conclusions

The work reported in this chapter has proposed a simple algorithm for extracting a real-time indicator of system stress from PMU data. While the nature of the power system problem is such that the exact use and interpretation of the algorithm's output are quite different, the basic computation is very close to the well-established use of Singular Value Decomposition (SVD) in Principal Component Analysis (PCA), The organization of PMU measurements, and the computation proposed is extremely simple. One simply constructs a matrix, in which each column is a stacked vector of the available PMU measurements over a time window, with the most recently acquired measurements comprising the right-most column, the "oldest" measurements comprising the left-most column. The recommended window length is a number of samples equal to 2 to 3 times the number of available PMU measurements. One then simply computes and tracks the largest singular value of the matrix, updating at each sampling instant with the newly acquired vector of measurements. This computation is wholly measurement based, and may be termed a "model free" analysis.

Based on underlying geometric properties of the SVD, and the relation between time varying power systems loads/injections and measured voltage phasor magnitudes and angles, this largest singular value computed from measurement data may be hypothesized to approximately track the largest singular value of the inverse power flow Jacobian. Numerical studies in IEEE test systems suggest that this hypothesis is very accurate when a complete set PMU measurements are available for every bus, and remains reasonable accurate in more realistic PMU penetration levels of slightly less than 10%.

Large magnitude for the maximum singular value of the power flow Jacobian inverse (or equivalently, approach to zero for the smallest singular value of the power flow Jacobian itself) has long been accepted as an indicator of operating point ill-conditioning, and

system vulnerability to voltage instability. Hence, given that the SVD-based PMU measure approximately tracks this maximum singular value of the power flow Jacobian inverse, *without the requirement for any of the data needed to compute the Jacobian,* this work has succeeded in its initial goal of providing a model free indicator of system stress computed from PMU measurements.

With this new framework established, many avenues for future work remain. As in traditional PCA algorithms, data scaling and bad data filtering are significant practical issues to be addressed. Likewise, more careful analytic study of optimal window size needs to be addressed, to improve upon the heuristics developed to date (window size 2-to-3 times measurement vector size). More complete use of the information available in the singular vectors of the $\boldsymbol{U}$ and $\boldsymbol{V}$ unitary matrices requires exploration. Most significant may be the need to explore algorithms for calibrating the threshold of the SVD-based measure that would alert operators of the need for corrective action. Such algorithms will likely be based in part on off-line studies comparing to full-information calculation of the power flow Jacobian, as have been initial explored in this report, but may also benefit from use of statistical learning techniques over historical data sets.

3. PMU Enhanced Power Flow Solutions

3.1 Background

Phasor measurements units (PMUs) are beginning to be widely deployed in electric power systems, with this trend expected to continue, partially as a result of recent U.S. Department of Energy (DOE) smart grid funding. However even with this increase in the number of installations, PMUs will still only deployed at a small percentage of system buses for at least a number of years. This presents a challenge: how to get useful information from this small number of data points.

The key driver for PMU technology is the application of the precise time sources provided by GPS (Global Positioning System) satellites to accurately measure the relative voltage and current phase angles at buses across an interconnect. While there is currently significant interest in the application of PMUs, the key ideas themselves are not new, with a paper from 1980 [8] indicating how the then new GPS system could provide precise time sources, and a paper from 1983 showing how this information could be used to accurately obtain power system phase angles [9] across a wide area. An interesting history of PMU applications is provided in [10].

This characteristic of being able to directly measure the phase angles across an interconnected power grid is a key advantage that PMUs have over SCADA (with the other advantage being the much faster PMU sampling rate). The focus of this section is on the direct use of these bus phase angles within the power flow (quasi-steady state) time frame.

One well known application of the PMU bus phase angles is within the state estimator (SE). The use of these measurements in the state estimator was first described in 1986 [11]. The application of PMU values in SE continues to be an active area of research, with [12], [13], [14], and [15] several examples of this work.

In contrast, this section describes how PMUs value can be utilized in an operational and/or analysis context beyond their use in SE. The motivation for this application arises because in a variety of situations SE results may not be available. For example, smaller utility control systems may not have an SE, the SE may have failed to converge during rapidly changing system conditions, there may be a need to combine SE results with a larger system model, or people involved in nonoperational aspects of the power grid, such as marketers and power system planners, may not have access to SE results. But often a power flow case is available that at least approximates (to some degree) the current operating condition.

3.2 The Global Properties of Bus Phase Angles

Most power system measurements provide a localized view of the conditions on the electric grid. For example, a bus voltage magnitude measurement tells the voltage at a particular bus, while a line flow measurement tells the flow on a particular line. While these values can sometimes be used to infer information about system conditions one or two buses away, they certainly do not provide any global information. However, as will be shown here such information is provided by the bus phase angles.

For simplicity the remainder of section utilizes the dc power flow approach [16, pp. 75]. The dc power flow greatly simplifies the power flow by making a number of approximations including 1) completely ignoring the reactive power balance equations, 2) assuming all voltage magnitudes are identically one per unit, 3) ignoring line losses, and 4) ignoring tap dependence in the transformer reactances. Hence the dc power flow reduces the power flow problem to a set of linear equations

$$\mathbf{P} = \mathbf{B}\ \theta \tag{3.1}$$

where **P** is the vector of bus real power injections, **B** is bus susceptance matrix, and θ is the vector of bus voltage angles. Since the equations are linear they always have a single solution, which can be directly calculated by solving

$$\theta = [\mathbf{B}]^{-1}\ \mathbf{P} \tag{3.2}$$

eliminating the need for iterations. While the dc power flow is certainly an approximation, it often provides reasonable results with respect to the real power flows in a system [17],[18], [19].

What is clear from (3.2) is when using the dc power flow approximation the angle at any bus the system is an linear combination of the power injections at all the buses in the system. Note that while **B** is sparse, its inverse is not. Also recall that in a power flow bus phase angles are also specified with respect to the system slack bus, where the slack bus angle is usually assumed to be 0.

To get a feel for the magnitude of a bus angle's dependence on the power injections throughout the system, Figure 3.1 contours the bus phase angle to power injection sensitivities for the Wempleton 345 kV bus, located in Northern Illinois, using a 43,000 bus model. The sensitivities are in degrees/per unit power injection using a 100 MVA base. Hence the figure is showing the values of one row of the inverse of the **B** matrix. The interesting result is that most locations matter, with sensitivities at many system buses a significant fraction of the values at Wempleton itself. The only locations with zero sensitivity are the system slack bus (Brown's Ferry in Northern Alabama), and buses that are not part of the interconnect, such as Quebec. Therefore any power transaction between buses with different sensitivity values will be reflected in the Wempleton bus angle, indicating it is providing global information about the system state.

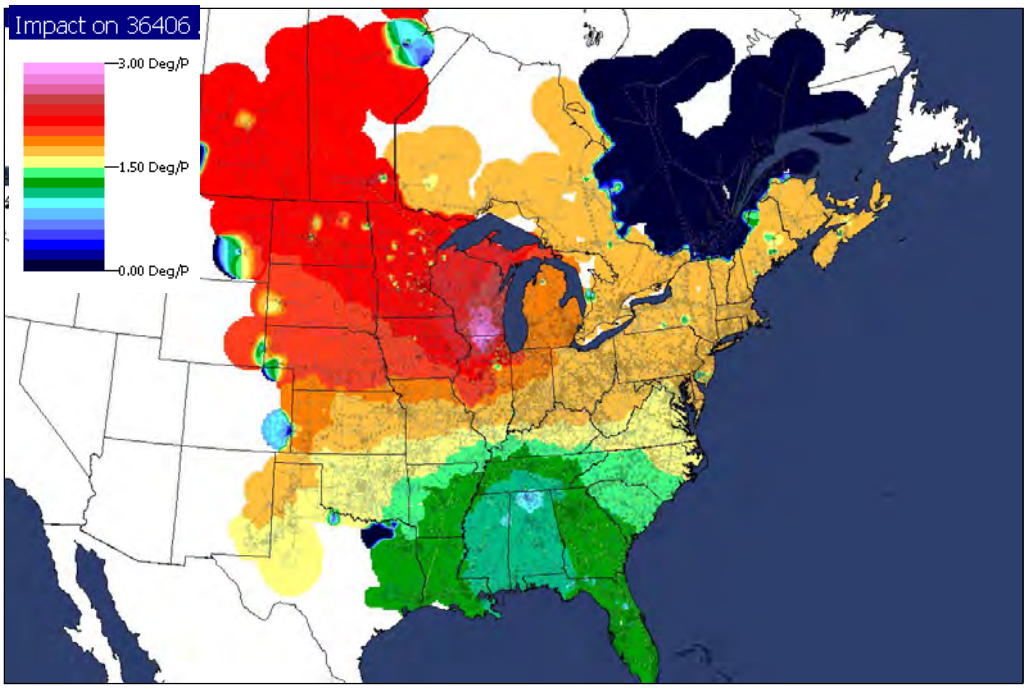

Figure 3.1 Dependence of Wempleton 345 kV bus angle (in Northern Illinois) on power injections throughout the Eastern Interconnect

The flipside of this widespread dependence is that the problem of trying to estimate a particular bus injection based on a single phase angle measurement is completely under-determined. However as the focus shifts from looking at a single phase angle to looking at phase angle differences, the phase angle difference to power injection sensitivities become more localized. For example, Figure 3.2 contours the sensitivities of the angle difference between two buses located on different sides of the Chicago Metro region (the Wempleton and Burnham 345 kV buses) to the power injections throughout the Eastern Interconnect. Hence the figure is showing the different between two rows in the $[\mathbf{B}]^{-1}$ matrix. Note the change in the contour scale from between 0 and 3 degrees for Figure 3.1 and between -1 and 1 degrees for Figure 3.1, with most of the Figure 3.2 values very close to zero. Figure 3.3 shows a zoomed view of the Figure 3.2 results; the location of the Wempleton bus is indicated by the high sensitivity values close to the Illinois/Wisconsin border, whereas Burnham is located near the bottom of Lake Michigan, close to the Illinois/Indiana border.

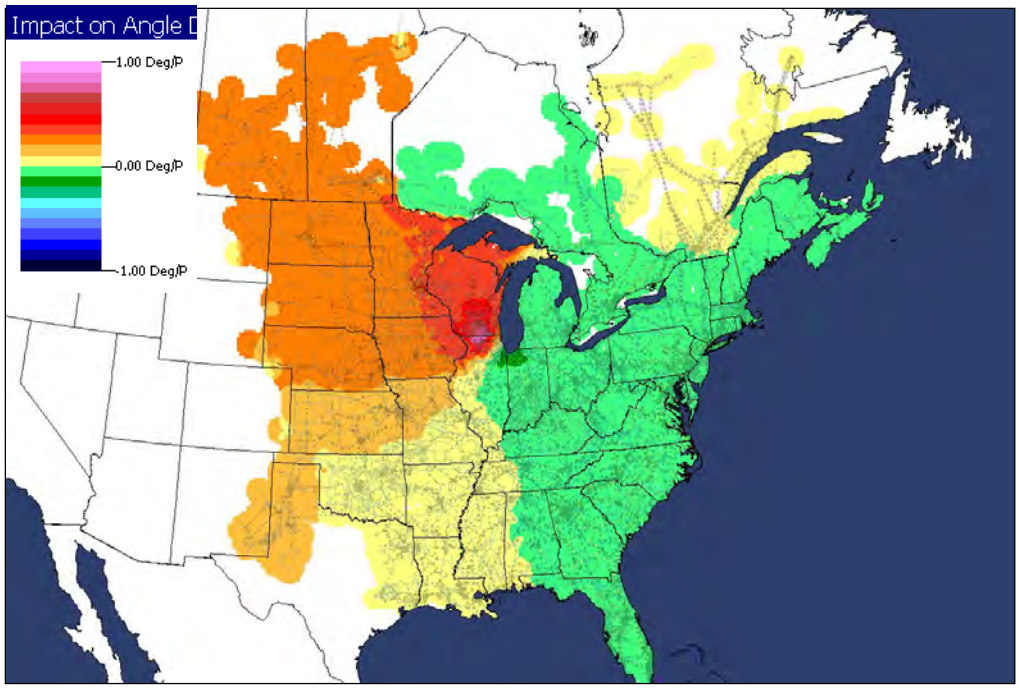

Figure 3.2 Dependence of phase angle difference between the Wempleton and Burnham 345 kV bus angles (in Northern Illinois) on power injections throughout the Eastern Interconnect

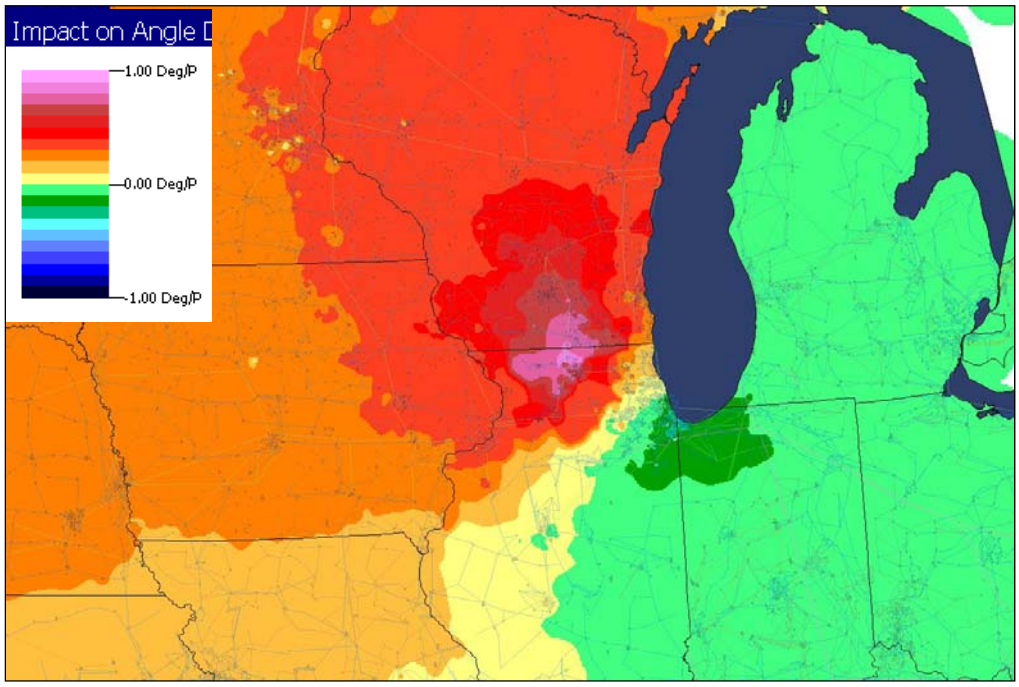

Figure 3.3 Zoomed view of Wempleton to Burnham phase angle difference sensitivities

While the phase angle difference between just two buses can say very little about the injection at a particular bus, what does become apparent from Figure 3.2 and Figure 3.3 is that such values could be used to get at least a qualitative feel for the net power flows between regions. For example, if the upper Midwest is exporting power to the rest of the Eastern Interconnect this will probably be indicated by a higher phase angle difference between Wempleton and Burnham. Expanding this concept to more bus angle measurements, the premise is that these measurements can be used to modify an existing power flow solution to better match a particular operating point. This idea is presented next.

3.3 PMU Morphed Power Flow Solutions

A common power system analysis task is to take an existing power flow case and then modify it to match a particular actual operating condition. This could be done in near real-time by an operations engineer for a utility without an SE, or it might be done days or months later by a market analyst trying to use publically available information, such as the FERC 714 data that tells hourly control area loads, to recreate the operating conditions of perhaps an entire interconnected system.

A typical approach to accomplish this is to take a power flow case with branch statuses, and a load and generation profile that at least approximates matches the desired system operating point, and then modify the total loads for desired areas based upon the actual dispatch, change the statuses of important branches to match their actual values, and then set the outputs of important generators. However, because of the time consuming nature of this task, it is usually only done for a small portion of the entire system. What is often lacking in this approach at good estimates for the net power interchange.

Here we propose to augment this process to include PMU values. Of course from a SE perspective just using a handful of PMU values to try to estimate an entire power system operating point results in a hopelessly under-determined problem. But if one starts with a solved power flow, and then uses the small number of measurements to better estimate the operating point associated with the measurements, the problem is amendable to an application of an linear programming (LP) based optimal power flow (OPF) algorithm.

The OPF algorithm, which was first formulated in the 1960's [20], [21], involves the minimization of some objective function subject to a number of equality and inequality constraints:

$$\begin{aligned} &\text{Minimize } F(\mathbf{x},\mathbf{u}) \\ &\text{s.t. } \mathbf{g}(\mathbf{x},\mathbf{u}) = \mathbf{0} \\ &\mathbf{h}_{\mathbf{min}} \le \mathbf{h}(\mathbf{x},\mathbf{u}) \le \mathbf{h}_{\mathbf{max}} \\ &\mathbf{u}_{\min} \le \mathbf{u} \le \mathbf{u}_{\max} \end{aligned} \tag{3.3}$$

where **x** is a vector of the dependent variables (such as the bus voltage magnitudes and angles), **u** is a vector of the control variables, $F(\mathbf{x},\mathbf{u})$ is the scalar objective function, $\mathbf{g}(\mathbf{x},\mathbf{u})$ is the set of equality constraints (e.g., the power flow equations), and $\mathbf{h}(\mathbf{x},\mathbf{u})$ is the set of inequality constraints.

Over the years several different OPF solution approaches have been proposed, with an excellent literature survey recently presented in [22] and a tutorial in [23]. These

approaches can be broadly classified as either linear programming (LP) based methods or non-linear programming based methods. The algorithm utilized here is based upon the LP approach [24].

Overall for a full ac system model the LP OPF algorithm iterates between solving the power flow to determine the power system violations, with an LP using a linearized model of system constraints to redispatch the control variables subject to certain equality and inequality constraints. The key to the computational efficiency of the LP itself is to minimize the number of constraints included in the LP tableau. Practically all the constraints of (3.3) are considered by either enforcing them using the power flow or, in the case of most nonbonding inequality constraints, monitoring but not enforcing them as long as they remain nonbonding.

In the PMU morphed power flow approach presented here the set of binding constraints is setup to include the PMU bus angle measurements as equality constraints. Known system values, such as the output of generators or total area load, are treated as constants. Generators whose outputs are not known are treated as controls, as are the total area loads for areas without known values.

For the main optimization the LP itself utilizes a primal simplex algorithm with explicitly bounded variables [25]:

$$\begin{aligned} &\text{Minimize } \mathbf{c}^T\mathbf{u} \\ &\text{s.t. } \mathbf{Au} = \mathbf{b} \\ &\mathbf{u}_{min} \le \mathbf{u} \le \mathbf{u}_{max} \end{aligned} \tag{3.4}$$

where **u** is the vector of control variables from (3.3) augmented to include the LP slack variables, **c** is the vector of the current control incremental costs, **A** contains the active constraints (primarily the measurement sensitivities), and **b** is the vector of measurements. Lack of feasibility is handled using the slack variable approach of [26]. The elements of each row in **A** can be calculated quite efficiently using the approach from [27].

Key to obtaining a reasonable solution is the selection of the control costs. One approach would be to use piecewise linear cost functions centered on the current control value to minimize the deviation from the power flow operating point. Such a curve is shown in Figure 3.4.

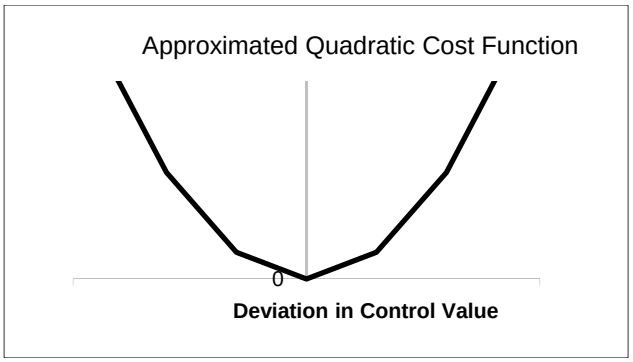

Figure 3.4 Piecewise linear cost function

As an initial motivating example, Figure 3.5 shows a three bus system in which all three lines have impedances of j0.1 per unit, with bus 1 as the system slack. Hence the **B** matrix is

$$\mathbf{B} = \begin{bmatrix} 20 & -10 \\ -10 & 20 \end{bmatrix}, \quad \mathbf{B}^{-1} = \begin{bmatrix} 0.0667 & 0.0333 \\ 0.0333 & 0.0667 \end{bmatrix} \tag{3.5}$$

and

$$\boldsymbol{\theta} = \begin{bmatrix} 20 & -10 \\ -10 & 20 \end{bmatrix}^{-1} \begin{bmatrix} 0.6 \\ -1.8 \end{bmatrix} = \begin{bmatrix} -0.02 \\ -0.1 \end{bmatrix} = \begin{bmatrix} -1.15\,\text{deg} \\ -5.73\,\text{deg} \end{bmatrix} \tag{3.6}$$

which matches the values shown in the figure.

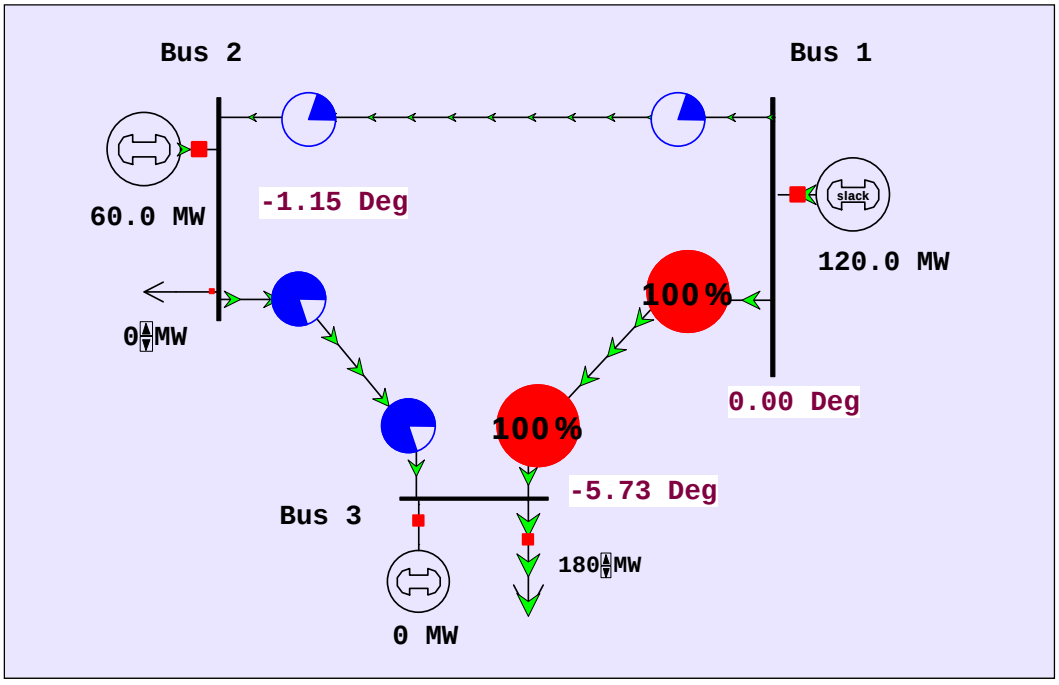

Figure 3.5 Three bus system

Now consider an under-determined problem with this same network. Assume the load is known, and that the bus 2 phase angle is known (with respect to the bus 1 slack angle of 0). The phase angle measurement introduces the constraint

$$P_{G2} * 0.0667 + (P_{G3} - 1.8) * 0.0333 = \theta_{2,meas} \quad (3.7)$$

This constraint would represent one row of **A** in (3.4). Another row of this matrix would be the power balance constraint

$$\Delta P_{G1} + \Delta P_{G2} + \Delta P_{G3} = 0 \quad (3.8)$$

This is a problem with three variables and two constraints, so an infinite number of solutions would give the specified phase angle. Nevertheless, the premise here is that by taking into account various power flow constraints, such as generator limits and (optionally) line flow constraints, it is possible to algorithmically morph the initial power flow into one that matches the measured angles.

As a large system example, Figure 3.6 shows the bus phase angle contour for Northern Illinois using a 13,000 Midwest system model. This represents the starting power flow solution.

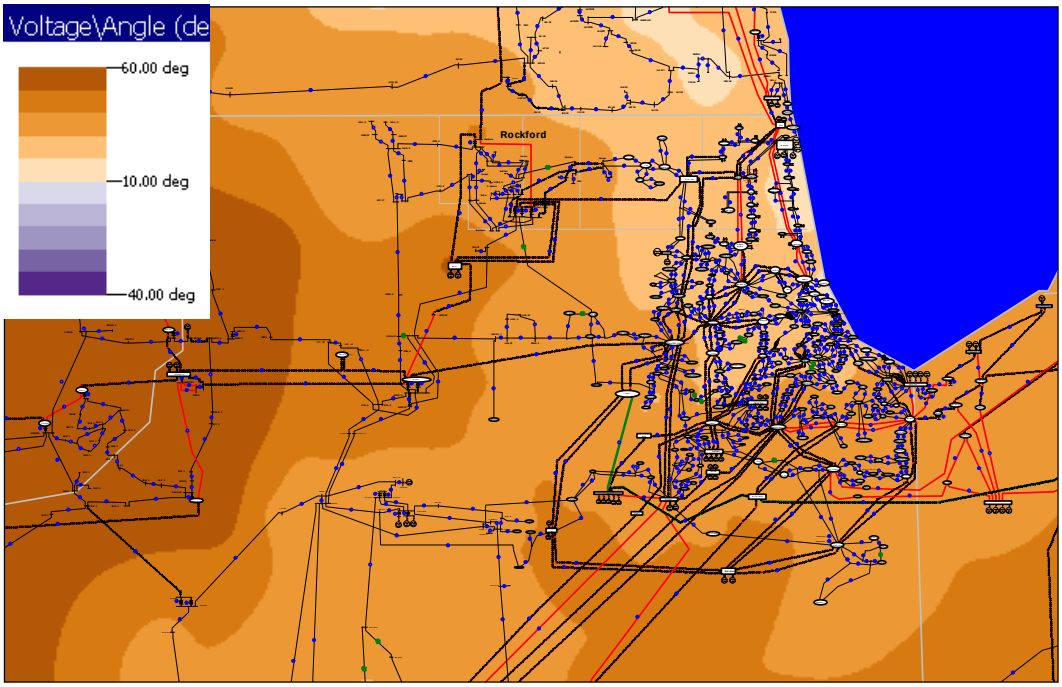

Figure 3.6 13,000 bus Midwest system angle contour before transaction

Next, the Figure 3.6 case was modified by setting up a 2000 MW transaction between the Northern Illinois (NI) area and the slack bus area (TVA). To implement the transaction the outputs of all the generators in NI were reduced using a participation factor approach, in which the generator participation factors were proportional to the rated MW capacity. This resulted in the new system operating point shown in Figure 3.7 13,000 bus Midwest system angle contour, with 2000 MW transaction to Slack Area

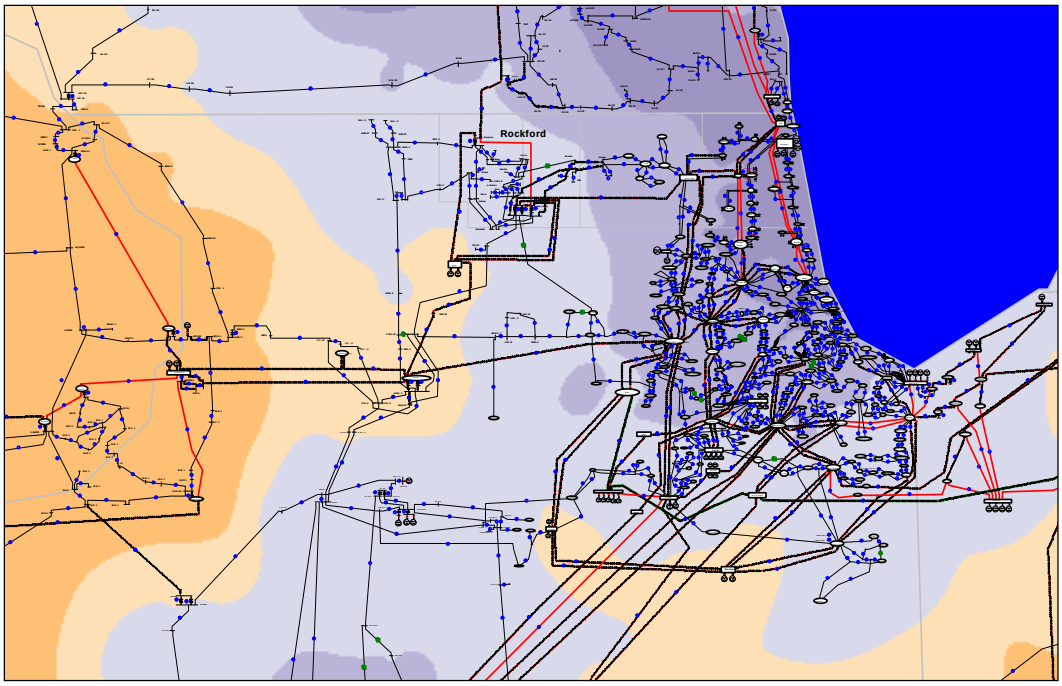

Figure 3.7 13,000 bus Midwest system angle contour, with 2000 MW transaction to Slack Area

To demonstrate the algorithm, the starting point was the Figure 3.6 operating point. Then the algorithm was applied using four angle measurements from the Figure 3.7 operating point, and 25 generators set as controls. This resulted in the operating point shown in Figure 3.8 with the net NI interchange reduced by 1977 MWs. This change required 19 LP primal iterations. A comparison between Figure 3.7 and Figure 3.8 indicates the close agreement in the two solutions, at least at a macroscopic level.

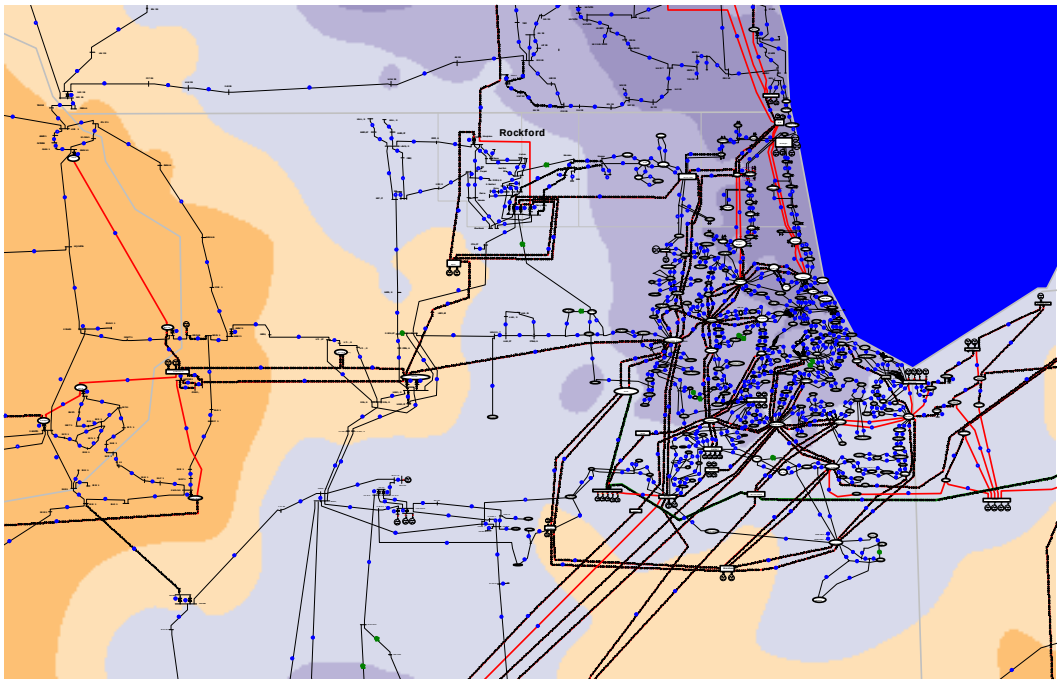

Figure 3.8 13,000 bus Midwest system angle contour, original case morphed using four angle measurements

4. Visualization of Oscillation Monitoring System Results

4.1 Background

Oscillation Monitoring System (OMS) is being developed at Washington State University (WSU) as a real-time operations toolbox for monitoring the damping ratio, frequency, as well as mode shape of poorly damped electromechnical oscillations in the power system from wide-area PMU measurements. OMS includes two engines as shown in the flowchart in Figure 4.1. Event analysis engine in Figure 4.1 carries out an automatic Prony type analysis of system responses during the occurrence of disturbances in the system. The complementary damping monitor engine in Figure 4.1 estimates the damping, frequency as well as mode shape of poorly damped oscillatory modes from ambient PMU measurements whenever such oscillations appear. Details on the two engines can be seen in [28], [29], [30].

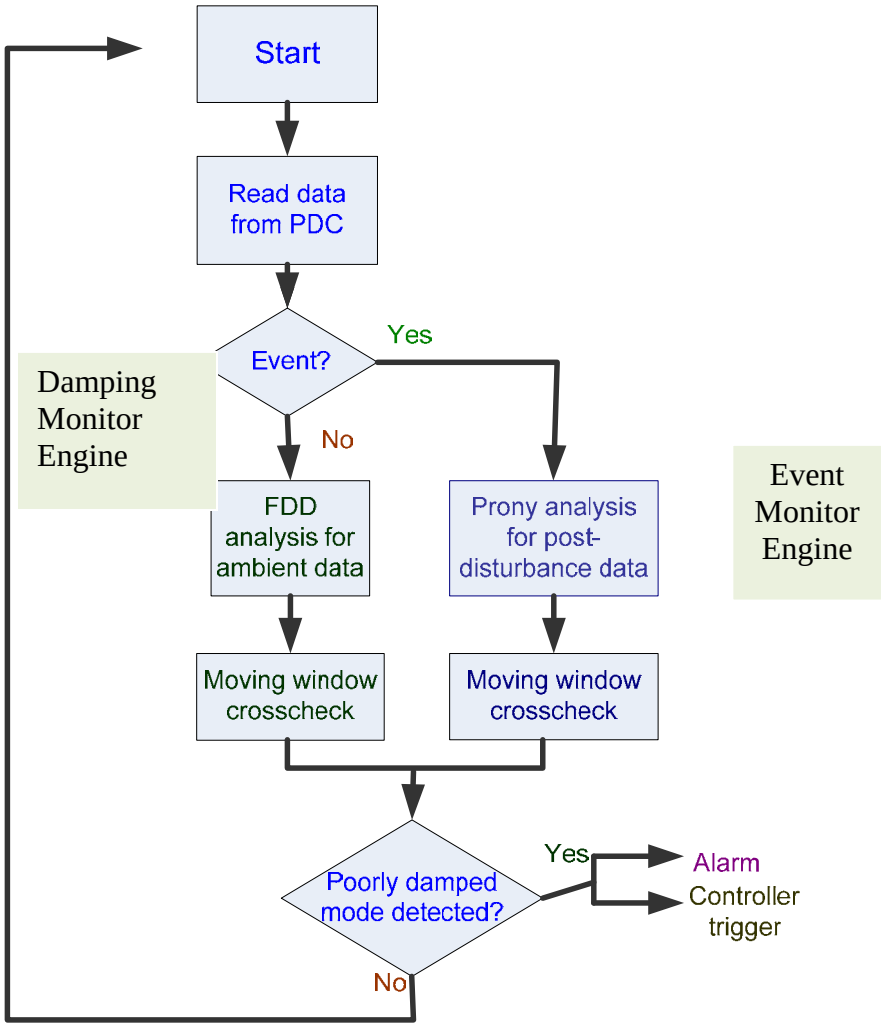

Figure 4.1: Flowchart of OMS

Figure 4.2 shows an example of the results from the two engines for a recent event near the Cumberland plant at TVA [31]. In Figure 4.2, the system encountered a routine event at about 830 seconds. The event analysis engine of OMS then carries out moving time-window analysis of the PMU measurements towards real-time Prony analysis and concludes the oscillation to be from a local mode (involving mainly one PMU or few nearby PMUs) of 1.2 Hz oscillations with +1.5% damping ratio. On the other hand, the damping monitor engine of OMS analyzes the real-time ambient PMU data continuously, and can estimate the dominant oscillatory mode to be the same local mode identified by Prony at 1.2 Hz with damping ratio of +1.8%. The two engines, namely, the event analysis engine and damping monitor engine serve as complementary engines in identifying the dominant poorly damped oscillatory modes of a power system whenever such modes exist.

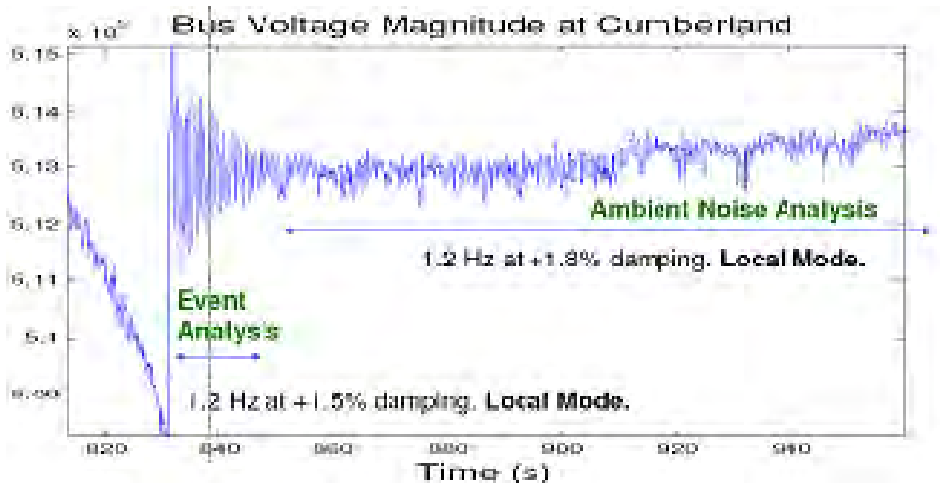

Figure 4.2 Illustration of OMS results from the two engines

4.2 Visualization of OMS Results

OMS has been implemented as an integral part of the Phasor Data Concentrator (PDC) at Tennessee Valley Authority (TVA) since 2008. The focus of the present PSERC project is to develop prototype visualization displays for showing the results of OMS onto secure web pages. Figure 4.3 shows information flow in the TVA OMS project. Whenever any of the two OMS engines gets a result, it is stored in the Results Database. Web server enquires results data from result database and refreshes the webpage, in a preset frequency (e.g., every 5 seconds). The changes will be shown on the remote client work station, and be available to system engineers and operators.

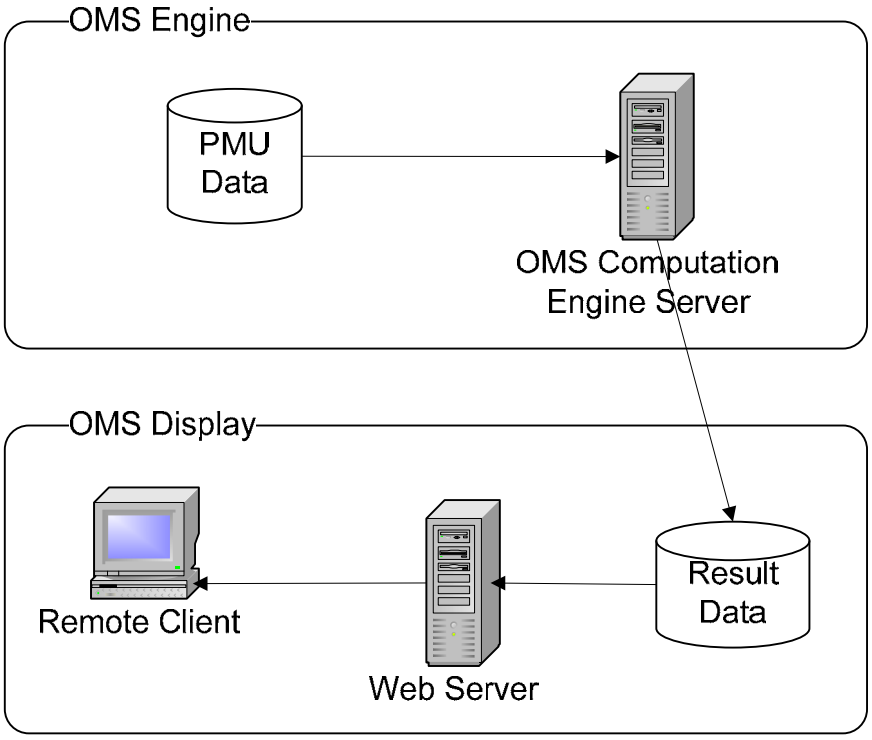

Figure 4.3 Data flow of OMS Project

Results Database

SQL database is used in this project. There are 7 tables in the results database: Event, Message, Message Source, Mode, Mode ID, Data Type, and Threshold. The information stored in each table is as follows:

Event: detected Events, or, large disturbances.
Threshold: various thresholds that are used to determine whether there is an event.
Message: reference information and error message.
Message Source: algorithm that generate this message.
Mode: OMS engine results, i.e. mode information, including frequency, damping ratio, mode shape amplitude, mode shape phase angle.
Data Type: defines the origin of result data: 1. Damping Monitor Detail, 2. Damping Monitor Consistent Result, 3. Event Monitor Prony Method Result, 4. Event Monitor Matrix Pencil Method Result, 5. Event Monitor HTLS Method Result, 6. Event Monitor Consistent Result.
Mode ID: defines the meaning of each mode ID. Mode ID is a three digit number. The left digit is Data Type, middle digit is mode number. The right digit defined as: 1. Frequency, 2. Damping Ratio, 3. Mode Shape Amplitude, 4. Mode Shape Phase Angle, 5. Flag for Damping monitor or Relative Energy for Event Monitor.

Webpage Generation

To generate a nice display and user friendly interface, ASP.NET and Microsoft Chart Control Tools are used in the webpage development. Background code is in C#.

Figure 4.4 shows an example of damping monitor webpage captured from the TVA implementation. In the damping monitor display, there are three major areas. Left top is a frequency vs. damping ratio point chart. It clearly shows all the modes in the frequency domain, and their damping ration on y-axis. If there is not consistent result for 5 minutes, average value is calculated and range is displayed as white bars. The right top corner shows the time and a brief summary, which includes the status of each mode. The summary will change color according to the status of each mode. Bottom is mode shape area, which shows mode shapes of up to 4 modes, in a radial fashion. Different colors represent different signals, and the legends are listed on the right side.

Figure 4.4 Snapshot example of a Damping Monitor webpage

Figure 4.5 shows an example of an event monitor webpage. In the event monitor display, there are two areas. Top area shows the mode frequency and damping ratio. Damping ratio is shown in a dial like chart. The color of each area shows whether the mode is safe, caution, alert or alarm. Thus, it is very intuitive and very easy for operators to have quite reactions, since in the case of event, everything happens in seconds. The bottom part shows the mode shape, as in the damping monitor webpage.

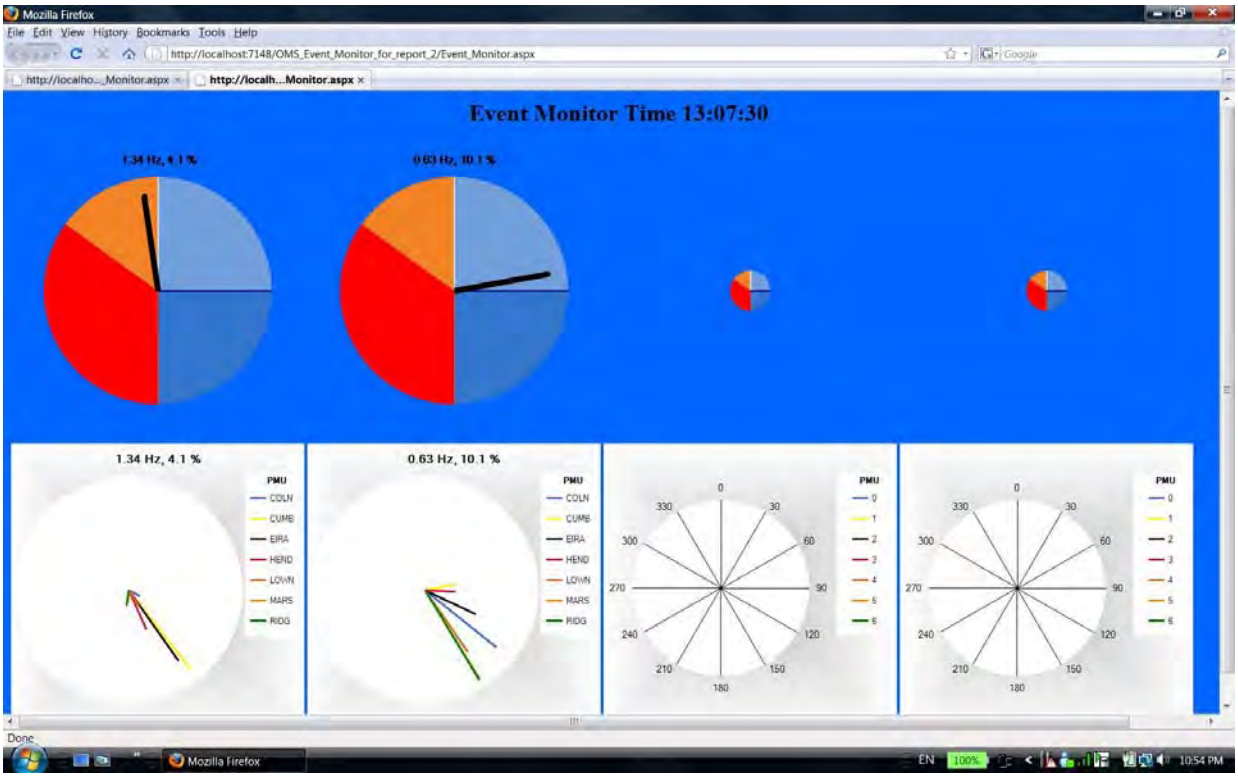

Figure 4.5 Snapshot of an Event Monitor webpage

5. Application of PMU Values for Improved Load Models

5.1 Background

Load representation has a significant impact on system stability analysis [32], [33]. Loads, in combination with other dynamics, are among the main contributors of low voltage conditions, voltage instability and even collapse in the power system. And it is becoming more evident that load model uncertainty is a major source of simulation inaccuracy for planning and operations. As transfer limits of the power flow are determined by such studies, load model accuracy is critical for maintaining the secure and economic operation of the power system. While scientifically accurate models have been proposed for generators, lines, transformers and control devices, the same has not occurred for load models because of the random and aggregate nature of a load composition.

There are two main approaches to developing load models: the physical component based approach and the measurement data based approach. We can determine the aggregate load model parameters if the parameters of all separate loads are well known. However, with the large number and types of loads connected at the transmission system level, such a physical component based approach to aggregate separate loads is numerically impractical. Therefore, in the absence of the precise information, we choose the measurement data based approach to obtain a reliable load model by implementing system identification techniques. This approach includes developing models with appropriate parameters and validating models with real-world response. Field measurements of voltage variations and the associated real and reactive power responses are required for the development and validation of the load models.

The load models also need to be updated in a timely manner to assure the best performance since the loads are actually evolving with time. While many papers discuss how to express the load model [34], [35], [36], there have been few attempts to develop a dynamic load model with variable parameters and to detect the parameter changes when there is no large disturbance and, hence, no big voltage variation. The final report of the August 14, 2003, blackout also indicated that one cause of the blackout was that the operators were using non-real-time data to support real-time operations [37]. As such, one focus of this work is to identify and update the load models with real-time data, so that more accurate reliability analysis can be performed in operations.

5.2 Overview of the Problem

Load models are mathematical representations typically relating power consumption to the voltage and/or frequency at a bus. Accurate load models are required to correctly evaluate the security (operational reliability) condition of a power system. Transmission power flow limits are determined from studies of these conditions. Accurate load modeling is essential to provide secure and economic planning and operation of a power system. Various static and dynamic models based on mathematical and physical representations have been studied to describe the overall load characteristics [38].

Classical static load models have been used in production-grade load flow programs for years. Common static load models for active and reactive power are expressed in a

polynomial or an exponential form, and can include, if necessary, a frequency dependence term [39]. But in recent years, several studies have shown the critical effect of load representation in voltage stability studies [38], [39] and therefore the idea of using static load models in stability analysis is changing in favor of dynamic load models.

Even though power system load has gained more attention, it is still considered one of the most uncertain and difficult components to model due to the large number of diverse load components, variable composition with time of day and week, weather and through time, and also because of lack of precise information on the composition of the load.

With the availability of phasor measurement units (PMU), we now can get access to the dynamic phenomena of electric power systems and form an improved load representation. In addition, the combination of the accurate load models with real-time updated parameters will help us decrease the uncertainty margin, resulting in a reliable and economic operation of the power system.

5.3 Load Models

Load models are classified mainly as static or dynamic. A static load model is not dependent on time, and therefore it describes the relation of the active and reactive power at any time with the voltage and/or frequency at the same instant of time. In contrast, a dynamic load model expresses this relation at any instant of time as a function of the voltage and/or frequency time history, including, typically, the present moment.

We can summarize the relation as:

$$\begin{aligned} P_t &= G_p(V_{0:t}, f_{0:t}, \theta_p) \\ Q_t &= G_q(V_{0:t}, f_{0:t}, \theta_q) \end{aligned} \tag{5.1}$$

where V and f are voltage and frequency, and θ is parameter set.

ZIP model or polynomial model

The static characteristics of the load can be classified into constant power, constant current and constant impedance load, depending on the relation of power to voltage. The ZIP model, (5.2), is a polynomial model that represents the sum of these three categories:

$$\begin{aligned} P &= a_p \left(\frac{V}{V_0}\right)^2 + b_p \left(\frac{V}{V_0}\right) + c_p \\ Q &= a_q \left(\frac{V}{V_0}\right)^2 + b_q \left(\frac{V}{V_0}\right) + c_q \end{aligned} \tag{5.2}$$

V_0 is the nominal value of the system for the study, and the coefficients a_p, b_p, c_p and a_q, b_q, c_q are the parameters of the model.

Exponential load model

Equation (5.3) expresses the power dependence on the voltage as an exponential function where the exponent is not restricted to 0, 1, or 2 as in the ZIP model.

$$P = P_l \left(\frac{V}{V_0}\right)^{\alpha_s}$$
$$Q = Q_l \left(\frac{V}{V_0}\right)^{\beta_s} \tag{5.3}$$

The parameters of this model are α_s, β_s, and the coefficients of the active and reactive power, P_l and Q_l.

Generic nonlinear dynamic load models

When the traditional static load models are not sufficient to represent the behavior of the load, a dynamic load model may be necessary.

In 1993 a popular dynamic load model was proposed by Hill in [], which captures the usual nonlinear steady-state behavior plus load recovery and overshoot. Other similar dynamic load models [] have been developed based on the same philosophy, steady-state behavior plus transients. Such load models are call generic nonlinear dynamic (GNLD) load models. We will adopt the exponential recovery dynamic load model from Hill's work.

The mathematical expression of the model is

$$\begin{aligned} P_d &= P_0 \left(\frac{V}{V_0}\right)^{\alpha_t} + z_p \\ T_p \dot{z_p} &= -z_p + P_0 \left(\frac{V}{V_0}\right)^{\alpha_s} - P_0 \left(\frac{V}{V_0}\right)^{\alpha_t} \\ Q_d &= Q_0 \left(\frac{V}{V_0}\right)^{\beta_t} + z_q \\ T_q \dot{z_q} &= -z_q + Q_0 \left(\frac{V}{V_0}\right)^{\beta_s} - Q_0 \left(\frac{V}{V_0}\right)^{\beta_t} \end{aligned} \tag{5.4}$$

where z_p and z_q are the corresponding recovery load states for real and reactive power, respectively; T_p and T_q are the load recovery time constants; P_d and Q_d are the real and reactive load power demands; and P_0, Q_0, and V_0 denote nominal real, reactive power, and voltage, respectively. The exponents α_s, α_t, β_s, and β_t stand for steady state and transient load-voltage dependences.

Equation (5.4) is the additive aggregate dynamic load model. Similarly, there is the multiplicative aggregate dynamic load model:

$$
\begin{aligned}
P_d &= z_p P_0 \left(\frac{V}{V_0}\right)^{\alpha_t} \\
T_p \dot{z_p} &= \left(\frac{V}{V_0}\right)^{\alpha_s} - z_p \left(\frac{V}{V_0}\right)^{\alpha_t} \\
Q_d &= z_q Q_0 \left(\frac{V}{V_0}\right)^{\beta_t} \\
T_q \dot{z_q} &= \left(\frac{V}{V_0}\right)^{\beta_s} - z_q \left(\frac{V}{V_0}\right)^{\beta_t}
\end{aligned}
\tag{5.5}
$$

Nonparametric load models

The nonparametric load models may consider the load or individual load components as a "black box," and transfer functions can be used to represent the load dynamics due to voltage variations.

The first-order linear dynamic load models can be characterized as functions of the change in system voltage

$$
\begin{aligned}
\Delta P_l &= \frac{k_{pv} + T_{pv} s}{T_{1p} s + 1} \Delta V \\
\Delta Q_l &= \frac{k_{qv} + T_{qv} s}{T_{1q} s + 1} \Delta V
\end{aligned}
\tag{5.6}
$$

where k and T are the load parameters for real or reactive power as functions of voltage depending on the subscript and T_1 is the time constant of the load.

Or we can use the difference equation:

$$
\begin{aligned}
\Delta P_l(k) &= \sum_{j=1}^{m_p} \sum_{i=1}^{n_p} a_{ij} \big(\Delta P_l(k-i)\big)^j + \sum_{j=1}^{m_{pv}} \sum_{i=1}^{n_{pv}} b_{ij} \big(\Delta V(k-i)\big)^j \\
\Delta Q_l(k) &= \sum_{j=1}^{m_q} \sum_{i=1}^{n_q} c_{ij} \big(\Delta Q_l(k-i)\big)^j + \sum_{j=1}^{m_{vq}} \sum_{i=1}^{n_{qv}} d_{ij} \big(\Delta V(k-i)\big)^j
\end{aligned}
\tag{5.7}
$$

Frequency dependent load models

Sometimes, the load model can also include frequency dependence, by multiplying the equations by the factor of the form:

$$
\begin{gathered}
\big[1 + K_p (f - f_0)\big] \\
\text{and } \big[1 + K_q (f - f_0)\big]
\end{gathered}
\tag{5.8}
$$

where f_0 and f are the nominal frequency and the frequency of the bus voltage, and the parameters K_p and K_q represent the frequency sensitivity of the model.

Augmented load models

Load models are not necessarily either static or dynamic. In fact, they are more likely to be a combination of both. We can use static models, either ZIP or exponential, augmented with dynamic ones to represent the loads

$$\begin{aligned} P &= P_s + P_d \\ Q &= Q_s + Q_d \end{aligned} \tag{5.9}$$

where P_s, Q_s are from Equation (5.2) or (5.3), and P_d, Q_d are from Equation (5.4) or (5.5). GNLD also belongs to this category.

Other widely used dynamic load models include the industrial load models (IM) using first or third or even higher order approximation for motors, or a combination of static and IM, such as [40], [41], [42]. A good summary of research and development in the area of load modeling can be found in [39].

5.4 Load Identification

The task of load modeling is in fact a system identification procedure. Two main approaches to develop the load models are the component-based approach and the measurement-based approach.

The component-based approach requires three sets of data

1. Load class mix data, which describe the percentage contribution of each of several load classes to the total active power load at the bus.
2. Load composition data, which describe the percentage contribution of each of several load components to the active power consumption of a particular load class.
3. Load characteristics data, which describe the electrical characteristics (e.g., power factor, voltage and frequency sensitivity) of each of the load components.

For an area whose load composition and characteristics will not vary widely, the component-based approach has the advantage of not requiring system measurements and therefore being more readily put into use.

For most systems, the loads are actually changing dramatically over time. Also, it is unrealistic to obtain all detailed individual components necessary for building the load model, not to mention the fact that it is impossible to update the data simultaneously. This work focuses on load modeling from a measurement-based approach.

The measurement-based approach uses system identification techniques to estimate a proper model and its parameters. The process of system identification involves finding a suitable model structure (mathematical model) and appropriate parameters for this structure that can replicate the dynamic response between change in voltage and corresponding changes in active and reactive powers.

The overall procedure (shown in Figure 2.4) used in this work is summarized as follows:

1. Data Acquisition
    a. Acquire measurement data (V, I, P, Q)
2. Voltage Detection
3. System Identification and Load Modeling
    a. Determine load structures to be used
    b. Identify which parameters can be estimated reliably from the available measurements
    c. Estimate parameters using a suitable method and an estimation criterion
    d. Validate the derived model
4. System Accepted

Our work is mainly in Step 2 and Step 3.

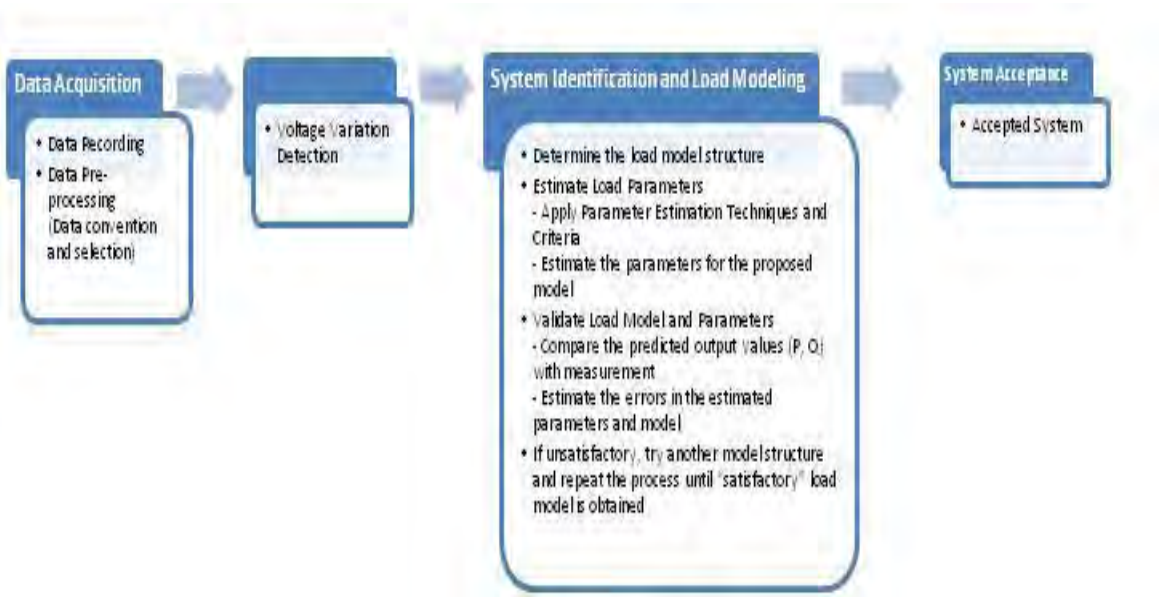

Figure 5.1 Load modeling procedure flow chart

5.4.1 Voltage variation detection

Since the data acquired contains mixed information, a procedure for detecting voltage variation must be applied before beginning the load identification process. We compare the incoming preprocessed data; if the voltage variation is in order of or greater than 1%, we open a new window and start the model identification process.

5.4.2 Load structure selection

Before engaging the complicated calculation, first we want to select a proper load structure to start with. Such selection could be based on the knowledge and experience of the system under study.

P-V relation

If no other information is available, we can identify whether static or dynamic load models are more suitable to describe the load with no complicated calculation or estimation, but, rather by inspecting the power-voltage relation and the first derivative of load power with respect to voltage.

Self-adjusted augmented model

Another approach to identify the load as static or dynamic is to use an augmented load model. If the dynamic part only accounts for a small portion, we can neglect the dynamic part and say the load is static. The results of this approach are illustrated in [].

5.4.3 Parameter estimation

After determining the right category of load model, the second step is to estimate parameters. That is, find a set of parameters for which the simulated results from proposed model best fit the measurement. In other words, find the optimal estimation of the parameters that minimizes the sum of the squares of the errors defined by

$$f(\theta) = \sum_{k} (\hat{y}_k(\theta) - y_k)^2 \tag{5.10}$$

where y_k is the actual (observed) power at time k, which would be the real and reactive power, $\hat{y}_k(\theta)$ is the given model prediction, and θ is the parameter vector that needs to be estimated.

Accompanying the development of different load models, various parameter estimation algorithms have been applied in identifying the models. Least-square methods are one of the most popular. Recently, more complex estimation techniques have been adopted in load model parameter estimation, such as genetic algorithms (Gas), simulated annealing (SA) and artificial neural networks (ANNs). The algorithm we choose here is the Levenberg-Marquardt algorithm (LMA). LMA is known for its robustness. Like other numeric minimization algorithms, LMA is an iterative procedure.

5.4.4 Load Model Validation

The derived parameter values need to be validated for their expected performance. The validation includes two steps: check the model quality on the identification data, and validate the model on a different set of measurement data.

For the first step, the load model output (response) is simulated and then compared with the measured output using the obtained parameter values. We evaluate the performance of the developed load model using the following relative error

$$\varepsilon_y = \sqrt{\frac{\frac{1}{n}\sum_{k=1}^{n}(\hat{y}_k - y_k)^2}{\frac{1}{n}\sum_{k=1}^{n}(y_k)^2}} \tag{5.11}$$

where y_k and $\hat{y}_k$ denote the measured and simulated (real or reactive) power, respectively. If ε_y is less than the desired threshold, say 1%, the dynamic load model is said to be acceptable.

If the performance achieved on the identification data is acceptable, the second step is to validate the model on a different set of measurement data, since parameter variance error could not be detected from the training data set. We need to choose identification data and measurement data carefully because the parameter is always time-varying.

5.5 Simulation Results

In this section, several cases with different load models are simulated using the automatic identification procedure. The voltage variation is detected to start the estimation process. Load type is determined both by inspecting the P-V relation and by using the self-augmented model. LMA is used to estimate model parameters. The identification data window is 3 s or until converge, whichever is larger. And the estimation results are validated by using the data after that until another voltage variation is detected.

Case 1: 3-Machine, 9-Bus System with PSS/E Static Load Model

The popular Western System Coordinating Council (WSCC) 3-machine, 9-bus system is used in the case study. Figure 2.6 is the one-line diagram of the system. PSS/E [43] was used to generate the data as a realistic simulation. The output of PSS/E was then used as the measurements for load identification. We use GENTRA for the machine model, IEEE1 for the exciter and TGOV1 for the governor. Both the static ZIP load model and static exponential load model are used in PSS/E simulation. Since we want to check the algorithm feasibility for updating time-variant parameters within normal operation conditions, we change the load parameters at times 5 s and 10 s, followed by a self-clearing fault at 15 s. The GNLD model is used, and if the dynamic term is detected to be negligible, it will self-adjust to static load model. Table 5.1 shows the estimation results for the ZIP load model.

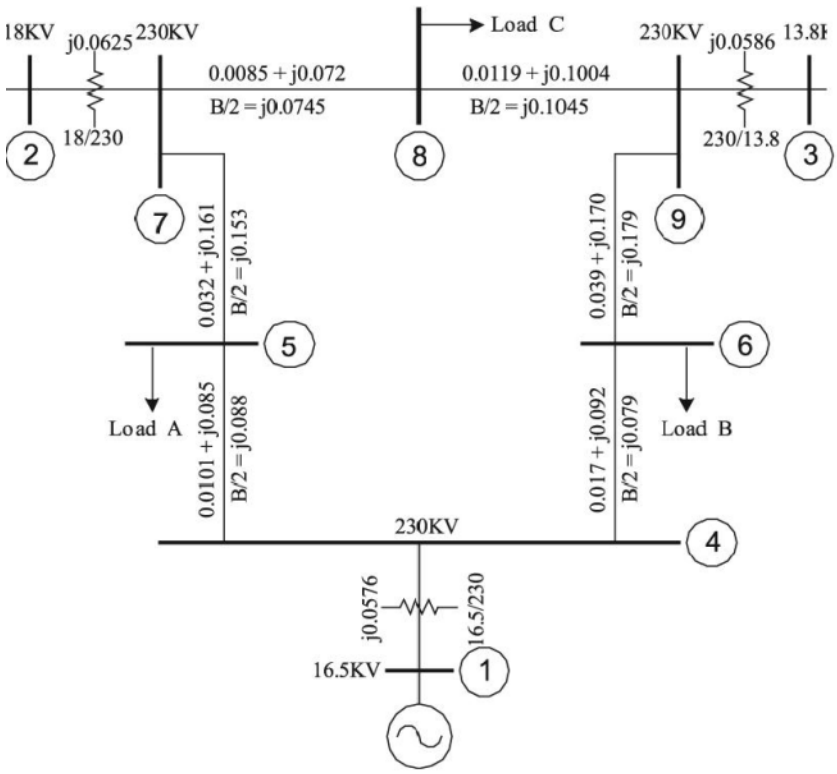

Figure 5.2 WSCC 3-machine, 9-bus systems

Table 5.1 ZIP Load Model Parameter Estimation

	Actual θ	**Estimated $\hat{\theta}$**	ε_θ	ε_P	L_w
Bus 5: 0-5s	[0.4413 0.5022 0.3125]	[0.4351 0.5146 0.3063]	3.4920e-3	3.5414e-8	45
5-10s	[0.4413 0.5022 0.5000]	[0.4256 0.5334 0.4845]	4.5820e-2	2.8082e-8	50
10-15s	[0.3500 0.6000 0.3000]	[0.3866 0.5268 0.3366]	1.1848e-1	3.5039e-8	43
15-20s	[0.3500 0.6000 0.3000]	[0.3498 0.6004 0.2998]	6.4751e-4	3.5048e-8	7
Bus 6: 0-5s	[0.3072 0.3555 0.2250]	[0.3062 0.3575 0.2240]	4.7931e-3	4.6258e-8	45
5-10s	[0.3072 0.3555 0.1000]	[0.3115 0.3467 0.1045]	2.2454e-4	5.5112e-8	39
10-15s	[0.3500 0.3000 0.2500]	[0.3403 0.3197 0.2400]	4.6063-2	4.7367e-8	5
15-20s	[0.3500 0.3000 0.2500]	[0.3501 0.2999 0.2501]	3.1011e-4	4.4943e-8	4
Bus 8: 0-5s	[0.3391 0.3937 0.2500]	[0.3387 0.3947 0.2495]	1.9867e-3	5.4609e-8	25
5-10s	[0.3391 0.3937 0.3000]	[0.3326 0.4070 0.2933]	2.2701e-2	5.2193e-8	43
10-15s	[0.2000 0.5000 0.3000]	[0.1947 0.5108 0.2945]	2.1531e-2	4.2135e-8	44
15-20s	[0.2000 0.5000 0.3000]	[0.2000 0.5001 0.3000]	1.7425e-4	6.2022e-8	7

$\theta = [a_p \quad b_p \quad c_p]$, and the initial value $\theta_0 = [0.3 \quad 0.3 \quad 0.3]$

Error is calculated as

$$\varepsilon_\theta = \sqrt{\frac{\frac{1}{p}\sum_{i=1}^{p}\left(\hat{\theta}_i - \theta_i\right)^2}{\frac{1}{p}\sum_{i=1}^{p}(\theta_i)^2}}$$
$$\varepsilon_P = \sqrt{\frac{\frac{1}{n}\sum_{k=1}^{n}\left(\hat{P}_k - P_k\right)^2}{\frac{1}{n}\sum_{k=1}^{n}(P_k)^2}} \tag{5.12}$$

where ε_θ is relative parameter error and ε_P is relative error of real power. L_w is the data length at which estimation starts to converge. Figure 5.3 shows the evolution of relative parameter error.

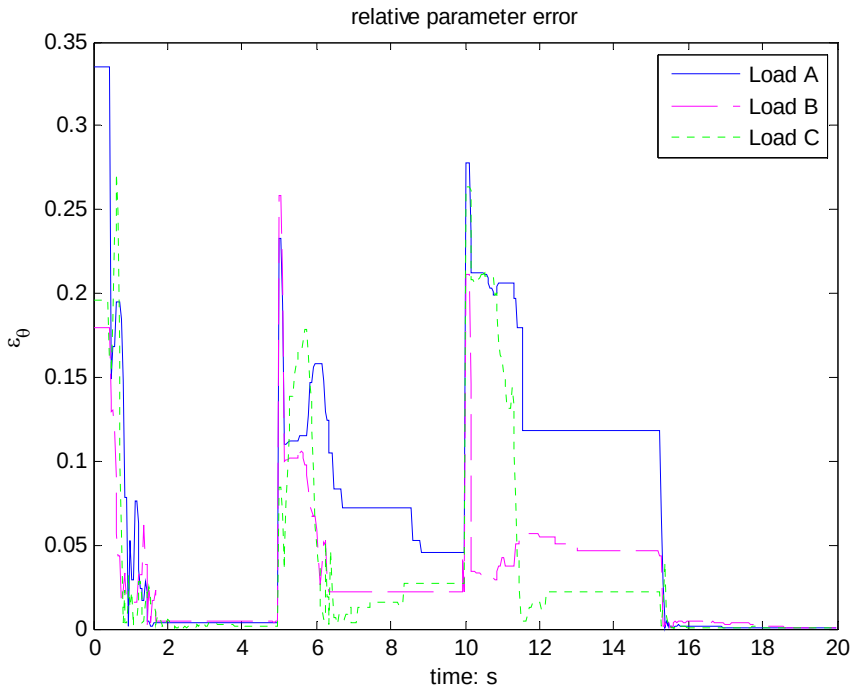

Figure 5.3 Relative parameter error for WSCC system with ZIP load model

Table 5.2 shows the estimation results for exponential load model, and Figure 2.8 is the relative parameter error.

Table 5.2 Exponential Load Model Parameter Estimation

	Actual θ	**Estimated $\hat{\theta}$**	ε_θ	ε_P	L_w
Bus 5: 0-5s	[1.2565 1.2]	[1.2566 1.2053]	3.0868e-3	1.6202e-5	50
5-10s	[1.5079 1.2]	[1.5079 1.2004]	2.0789e-4	2.5290e-5	10
Bus 6: 0-5s	[0.8844 1.4]	[0.8843 1.4028]	3.7736e-3	1.8826e-5	10
5-10s	[1.0809 1.4]	[1.0808 1.4003]	1.8176e-4	2.5407e-5	10
Bus 8: 0-5s	[0.9875 0.8]	[0.9874 0.8018]	1.4426e-3	1.0686e-5	34
5-10s	[0.5925 0.8]	[0.5925 0.7994]	5.0596e-4	1.8298e-5	6

$\theta = [P_l \quad \alpha_s]$, and the initial value $\theta_0 = [1 \quad 1]$

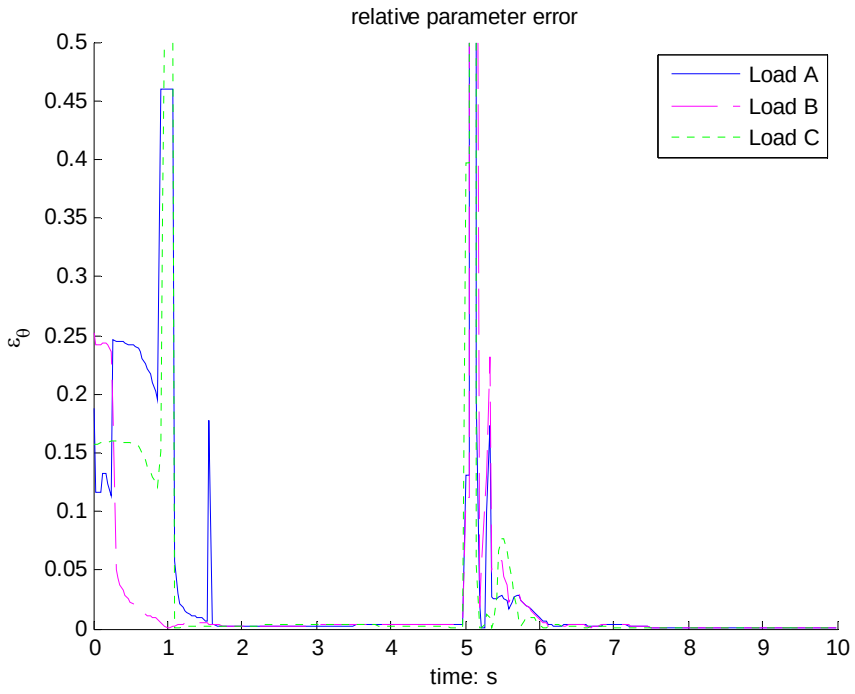

Figure 5.4 Relative parameter error for WSCC system with exponential load model.

Case 2: WSCC System with PST GNLD Load Model

Power System Toolbox [44] is modified to include the GNLD load model. Simulation is performed to obtain the data. We change the load parameters at time 10 s. Table 5.3 shows the estimation results for the GNLD model.

Table 5.3 GNLD Model Parameter Estimation

	Actual $\boldsymbol{\theta}$	**Estimated $\boldsymbol{\hat{\theta}}$**	$\boldsymbol{\varepsilon_\theta}$	$\boldsymbol{\varepsilon_P}$	$\boldsymbol{L_w}$
Bus 5: 0-10s	[1.25 1.2 5.0 0.5]	[1.2500 1.2000 5.000 0.5000]	3.6930e-11	2.0707e-11	9
10-20s	[1.35 1.3 6.0 0.6]	[1.3500 1.3000 6.000 0.6000]	3.9784e-11	4.5283e-13	28
$\theta = [P_l \quad \alpha_s \quad \alpha_t \quad T_p]$, and the initial value $\theta_0 = [1 \quad 1 \quad 2 \quad 0.2]$					

Nonparametric models are tested for this case. The difference models used are:

$$\Delta P_l(k) = \sum_{i=1}^{2} a_i \Delta P_l(k-i) + \sum_{j=1}^{2} \sum_{i=1}^{3} b_{ji} \left(\Delta V(k-i)\right)^j$$

It is shown that nonparametric model is a good approximation of the original load. But its performance is not as good as that of GNLD, so it will not be selected in this case. Table 5.4shows the estimation results using nonparametric model for GNLD load. Figure 2.9 is

the simulated results using estimation results of both GNLD and nonparametric models compared with measurement.

Table 5.4 GNLD Model Parameter Estimation

	Actual $\boldsymbol{\theta}$	**Estimated $\widehat{\boldsymbol{\theta}}$**	$\boldsymbol{\varepsilon_\theta}$	$\boldsymbol{\varepsilon_P}$
Bus 5:P 0-10s	N/A	[0.2644 0.6315 7.1740 0.1278 -7.0951 1.0311 1.0303 1.0295]	N/A	1.3538e-2
P10-20s	N/A	[0.9591 0.0151 3.1562 0.0654 -3.1614 1.0211 1.0221 1.0231]	N/A	2.6213e-3
$\theta = [a_1\ a_2\ b_{11}\ b_{12}\ b_{13}\ b_{21}\ b_{22}\ b_{23}]$, and the initial value $\theta_0 = [1\ 1\ 1\ 1\ 1\ 1\ 1\ 1]$.				

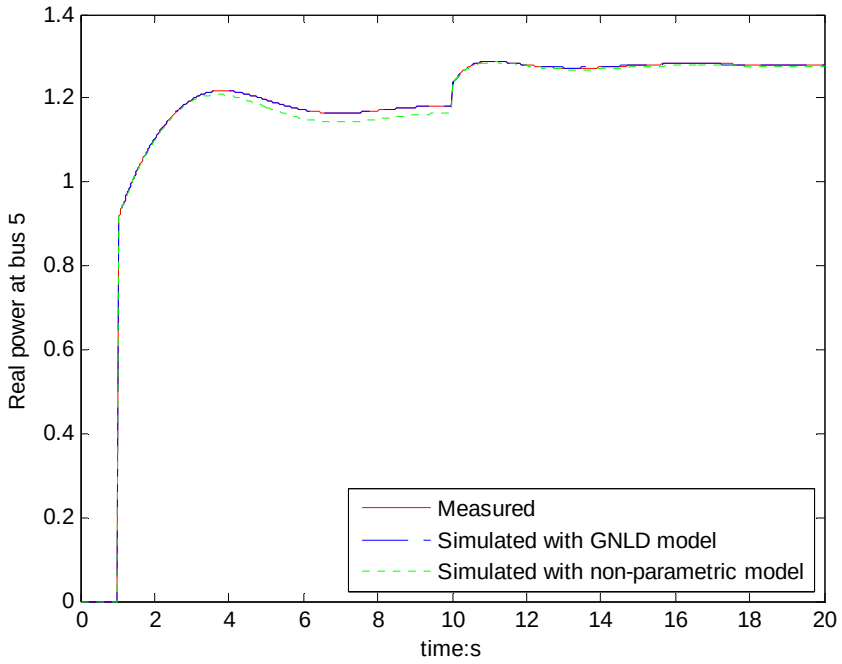

Figure 5.5 GNLD and nonparametric model simulated results compared with measurement.

Case 3: WSCC System with PSS/E Frequency Dependent Load Model
In this case, the model used in PSS/E has a frequency term for reactive power:

$$P = P_l \left(\frac{V}{V_0}\right)^{\alpha_s}$$
$$Q = Q_l \left(\frac{V}{V_0}\right)^{\beta_s} \times \left[1 + K_Q(f - f_0)\right] \tag{5.13}$$

Table 5.5 shows the estimation results.

Table 5.5 Exponential Load Model Parameter Estimation

	Actual θ	Estimated $\widehat{\theta}$	ε_θ	ε_P	L_w
Bus 5: P	[1.25 1.2 0.0]	[1.2500 1.2005 0.0087]	4.9658e-3	5.2693e-3	11
Q	[0.50 1.6 5.0]	[0.5000 1.6006 5.0123]	2.3094e-3	7.0196e-3	11
$\theta = [P_l \quad \alpha_s \quad K_P]$ or $[Q_l \quad \beta_s \quad K_Q]$, and the initial value $\theta_0 = [1 \quad 1 \quad 0]$					

Case 4: 30-Bus System using PowerWorld with Static Load Model

The 30-bus, 9-machine system with ZIP load model is used in PowerWorld. Figure 5.6 shows the one-line diagram of the system. Table 5.6 is the estimation results.

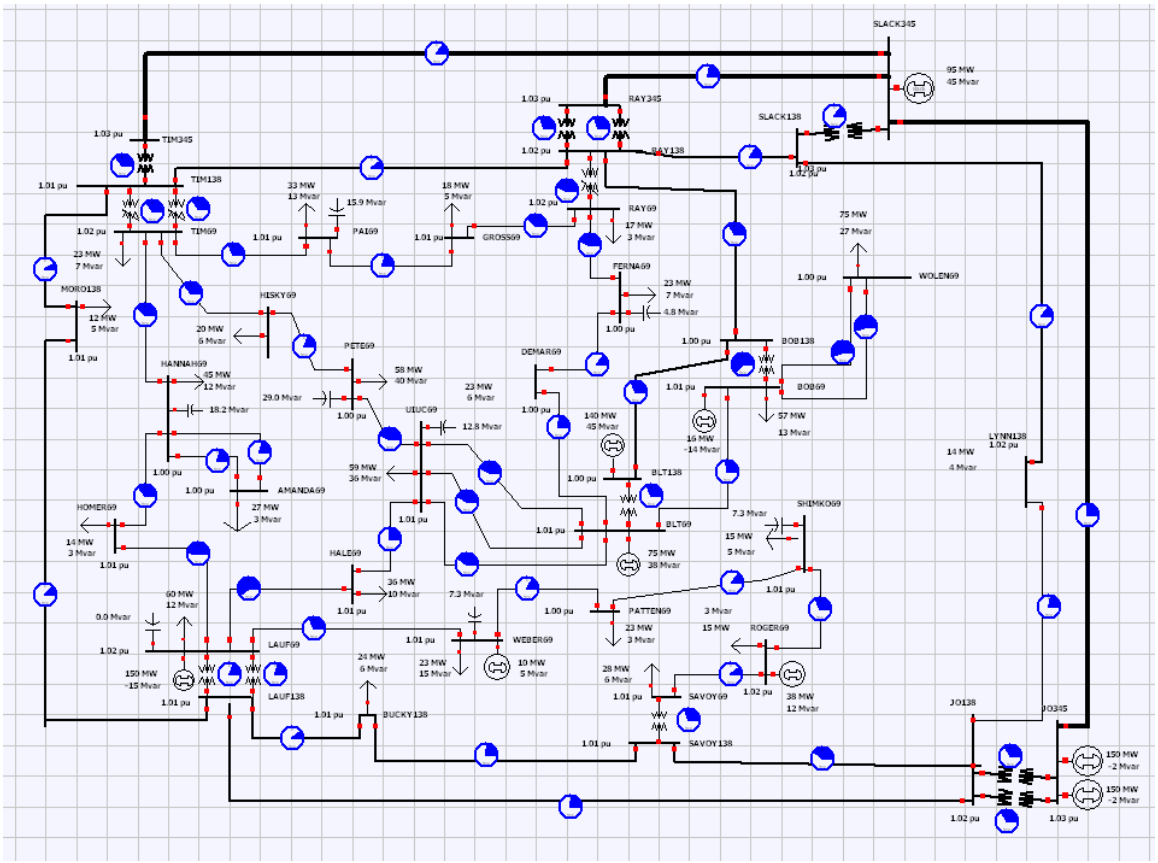

Figure 5.6 30-bus, 9-machine system

Table 5.6 ZIP Load Model Parameter Estimation

Bus	Actual θ	Estimated $\widehat{\theta}$	ε_θ	ε_P	L_w
3	[5.0 5.0 2.3]	[4.9995 5.0011 2.2995]	1.7680e-4	4.1222e-8	26
5	[5.0 5.0 4.0]	[4.9992 5.0017 3.9992]	2.4954e-4	4.1582e-8	18
10	[10.0 5.0 1.8]	[9.9988 5.0025 1.7987]	2.6961e-4	5.2461e-8	36
12	[10.0 10.0 2.9]	[9.9970 10.006 2.8970]	5.0878e-4	4.6082e-8	22
13	[0.0 20.0 3.0]	[-0.0050 20.0099 2.9951]	5.9773e-4	3.2200e-8	22
14	[20.0 0.0 2.2]	[19.9956 0.0086 2.1958]	5.2207e-4	3.7872e-8	5
15	[10.0 30.0 18.2]	[9.9960 30.0080 18.1960]	2.6683e-4	4.2821e-8	27
16	[20.0 10.0 27.8]	[20.0027 9.9946 27.8027]	1.8637e-4	3.7310e-8	11
17	[19.0 10.0 3.8]	[19.0103 9.9795 3.8103]	1.1541e-3	5.5814e-8	22
18	[0.0 0.0 45.0]	[0.0003 -0.0006 45.0003]	1.7057e-5	5.6805e-10	18
19	[8.0 2.0 8.3]	[8.0001 1.9998 8.3001]	2.5954e-5	3.4832e-8	22
20	[2.0 8.0 5.3]	[1.9992 8.0016 5.2992]	1.9802e-4	2.9231e-8	29
21	[20.0 30.0 24.4]	[20.0005 29.9991 24.4005]	2.6609e-5	3.2920e-8	22
24	[5.0 1.0 30.3]	[4.9973 1.0053 30.2973]	2.1302e-4	2.5281e-8	30
27	[0.0 0.0 20.0]	[-0.0002 0.0003 19.9998]	2.0724e-5	4.3467e-10	17
30	[9.0 1.0 13.4]	[9.0003 0.9994 13.4003]	4.8236e-5	3.0665e-8	22
33	[0.0 0.0 28.0]	[0.0011 -0.0022 28.0011]	9.4986e-5	4.1598e-10	32
34	[0.0 8.7 14.0]	[-0.0005 8.7009 13.9996]	6.6753e-5	2.1162e-8	18
37	[10.0 10.0 7.0]	[10.0007 9.9986 7.0007]	1.0578e-4	4.1939e-8	18
44	[9.0 0.8 50.0]	[9.0028 0.794350.0028]	1.3667e-4	3.0983e-8	23
48	[30.0 20.8 5.0]	[30.0056 20.7887 5.0057]	3.7634e-4	6.0972e-8	22
50	[10.0 3.0 1.1]	[10.0011 2.9978 1.1011]	2.5147e-4	6.5046e-8	53
53	[30.0 20.0 9.5]	[29.9936 20.0128 9.4936]	4.2070e-4	4.1011e-8	4
54	[10.0 0.0 2.43]	[9.9999 0.0002 2.4299]	1.9426e-5	4.8263e-8	27
55	[0.0 20.0 2.65]	[-0.0013 20.0026 2.6487]	1.5908e-4	2.5747e-8	13
56	[0.0 0.0 14.0]	[0.0018 -0.0037 14.0019]	6.6543e-2	1.3501e-9	35

$\theta = [a_p \quad b_p \quad c_p]$, and the initial value $\theta_0 = [3 \quad 3 \quad 3]$

6. Distributed Voltage Support on the Smart-Grid

6.1 Background

As PMU deployments become more common and their measurements become more available, there is greater real-time system observability. Improved monitoring motivates improved control, and this work examines a situation where end-user devices connected to the grid via inverters are used to provide reactive power support to the system. Devices such as solar panels and PHEVs are examples. More details of this work are available in [45] and [46] (also on the PSERC website). This research has shown how to determine effective locations in the transmission system and how to control reactive power resources at those locations. We also have considered how to determine reactive support groups which parallel the regions of the secure communications architecture that is presented. Ultimately, our goal is to present how the Smart Grid can allow the utilization of available end-user devices as a resource to mitigate power system problems such as voltage collapse.

6.2 Detect and Respond Framework

The reactive power capable devices, which may be located any place in the network, follow a chain of command structure analogous to the Incident Command System (ICS). In this system, actions are taken following a line of authority and responsibility. The ICS is a well-known, commonly-used, systematic tool for the command, control, and coordination of an emergency response. Personnel such as firefighters are a part of the ICS, and they use its framework to effectively manage an emergency situation such as a fire or a traffic accident to get the scene quickly under control. Recently, the oil well disaster oil in the Gulf of Mexico provides an example of an extremely large incident to which the response is coordinated using the ICS. Interestingly, a similar framework is needed for the intelligent control of reactive power control devices to respond efficiently when the power system is in crisis.

Applying this concept to power system devices, each individual reports to only one supervisor. The individuals work in groups and the group members report to a particular supervisor or officer who in turn reports to another specific officer. The individual end-user reactive-power-capable devices are the resources. Similarly to the personnel resources in the ICS, end-user devices do not normally work together, but they have the same goal in a crisis. An example of this hierarchical structure is shown in Figure 6.1.

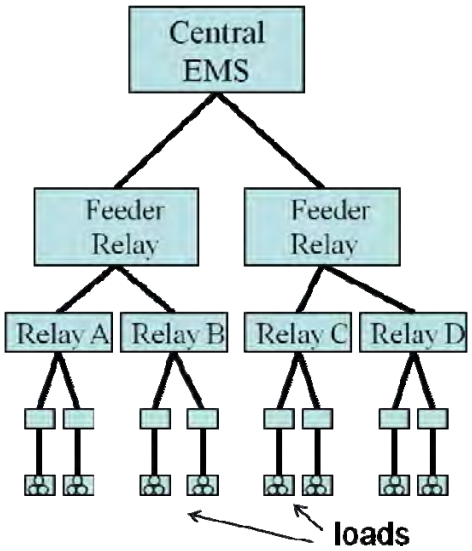

Figure 6.1 Hierarchical structure of reactive support system

Following the same structure, members of reactive support groups are responsible for assigning and coordinating the responses of those under their command. Distribution system buses and end-user devices also fall into this framework under the command of reactive support group members in the transmission system. The flowchart in Figure 6.2 illustrates the detection and response process in this system.

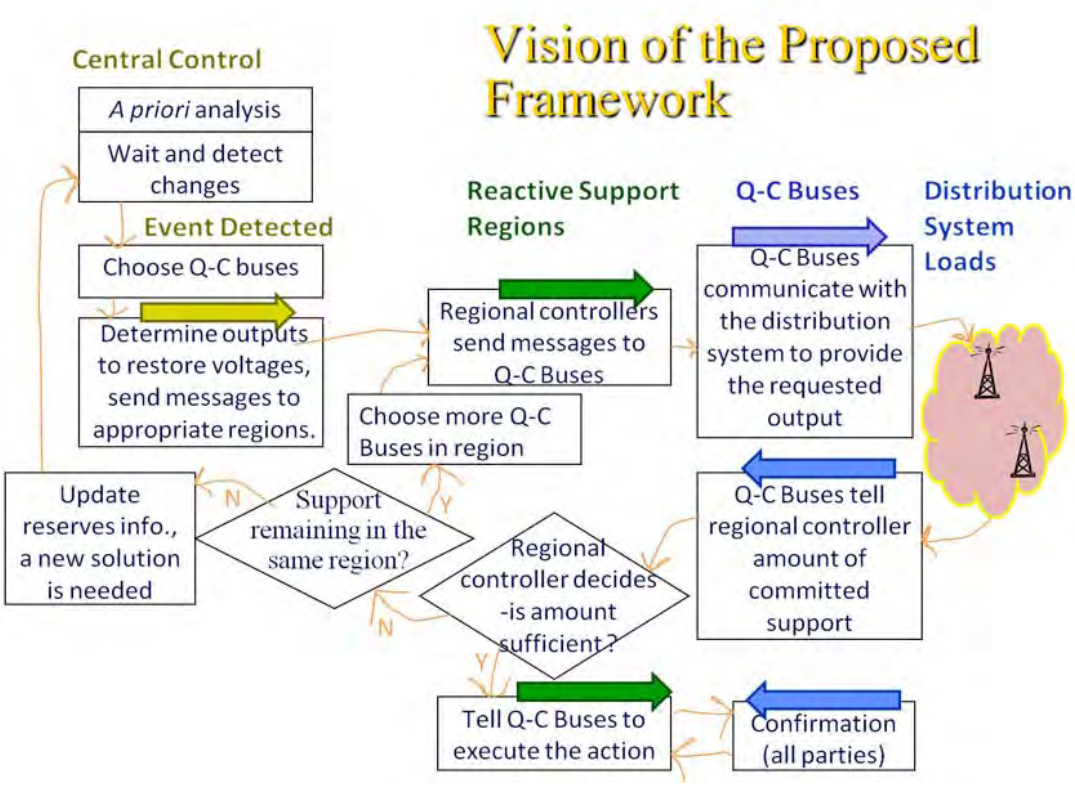

Figure 6.2 Flowchart of Detection and Response Framework

PMUs play an important role in the implementation of this framework. First of all PMUs are going to be instrumental in detecting voltage problems, which is the first step in initiating a response. Also, PMUs and other fast metering devices will also be important with respect to obtaining the most current information about the loads, both at the transmission system level and the distribution system level. A top-down detection-and-response pattern using this concept may work in the following way:

1. The Central EMS detects a voltage problem somewhere on the system. It computes a response that would mitigate the problem, using the approach described in this paper. It formulates action requests and sends them through the hierarchy where they are received by the feeder relays.
2. Each feeder relay receives a reactive support request which originated from the EMS. The feeder relay agent computes a set of response actions that would allow it to fulfill the request, formulates the corresponding action requests, and sends them to the relays to which they are connected.
3. Each relay receives the reactive support request from its feeder, computes a response action, formulates the corresponding action requests, and sends them to the load controllers it servers.
4. Each controller then controls the loads under its supervision to meet the requests.

These four types of communications and their accompanying responses each occur within a distinct realm. Each realm uses its own security parameters to deliver messages in a

timely way while ensuring secure exchange for its communicating partners. Key security requirements for this system as well as the potential solutions for providing an authenticated voltage control framework are discussed in [45] and [46].

6.3 Distributed Reactive Power

In this work, the only control actions considered are the injection of reactive power by end-user resources such as inverters, but such a scheme can be used to enact any corrective and preventative controls from other types of resources. A reactive power control example is shown using the IEEE 24-Bus Reliability Test System (RTS) (Figure 6.3) which has low voltages around 0.95 per unit. The lowest voltages in the system are at buses 3,4,8,9, and 24.

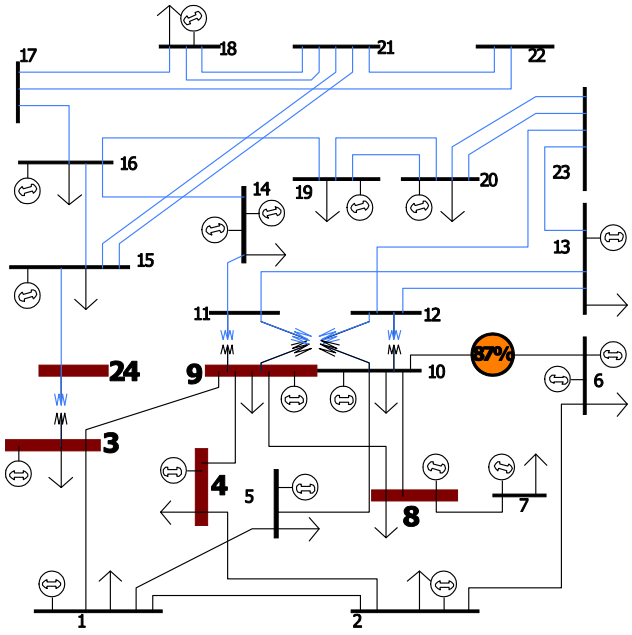

Figure 6.3. IEEE 24-bus RTS

Before control can be done, the controllability of the reactive component of loads must be classified. Initially, a load category can be assigned to each load based on prior knowledge, perhaps provided by the manufacturer or by the engineer performing the analysis, but these load categories will change over time and must be kept current. We define a Q-C bus as a bus which is selected to provide reactive power support. Classification incorporates knowledge about differing levels of reactive power control capability, and this helps select Q-C buses. In addition, selection of Q-C buses is based on sensitivities. The successfulness of this framework depends on having valid capability information about the available resources. To properly obtain the reactive power capabilities of Q-C buses, we must take high-quality measurements which are often reported back.

For the RTS, we define the category “CAT1” to contain the loads which are completely controllable, and “CAT3” to contain the loads which are not controllable at all. It is assumed that there are no partially-controllable loads at this time. Buses 11, 12, and 17

have reactive power loads of zero, so they are considered to be “CAT3” buses. The slack bus and the PV buses are also considered as “CAT3” buses since the reactive power output cannot be specified.

Using sensitivities and these load classifications, the five Q-C buses in the first column of Table 6.1 are obtained for the RTS. The value needed at each of these buses in order to make the voltage profile at the low-voltage buses within a tolerance of 1 per unit is determined, as shown in the second column of Table 6.1. Then, these adjustments are made in the system and the initial and final voltages are recorded in the third column of Table 6.1. Figure 6.4 shows the system voltages before and after the corrective action.

Table 6.1. RTS Voltage Improvement

Bus #	Initial Q_{net}	Final Q_{net}	Initial voltage	Final voltage
3	-37 MVAr	37 MVAr	0.9469	1.0057
4	-15 MVAr	15 MVAr	0.9598	1.0022
8	-35 MVAr	35 MVAr	0.9593	0.9975
9	-36 MVAr	36 MVAr	0.9603	1.0050
24			0.9594	0.9852

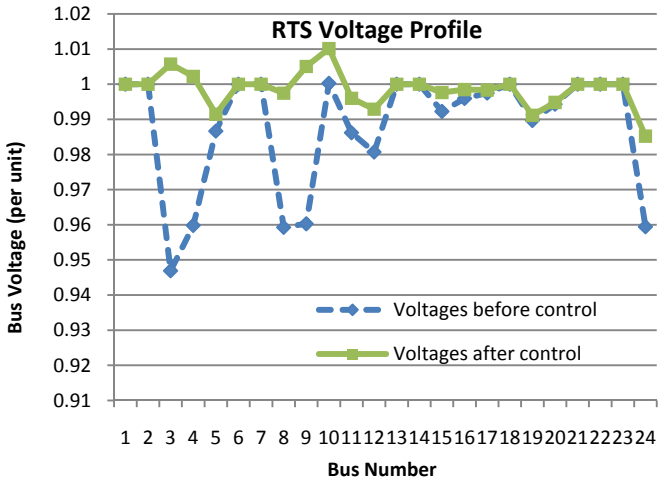

Figure 6.4. RTS voltage profiles

The use of reactive-only controls as opposed to other forms of corrective control has the advantage that such controllers are already available in the system but are not being utilized, and more are likely to be added, especially as the use of power electronics in homes increases. Also, the use of reactive power controls may prevent the need to shed load or change generation output as a corrective control.

In this example, the five worst voltages completely overlap the four most effective “CAT1” locations. As systems become more heavily loaded, the two groups will likely no longer overlap, as the lowest-voltage buses will no longer be “CAT1” because they will no longer have reserves. Furthermore, at high load levels, the response will likely no

longer be so linear, making it more difficult to determine the proper size for the adjustments. A comparison of control using linear estimates of Q_{net} to the actual required values of Q_{net} is given in [46] or the RTS.

Since reactive power support is local in nature and must be generated close to its point of consumption, such reactive power support must come from within the region with the voltage problems. These regions are called reactive support groups. Reactive support groups are buses chosen a priori to help each other. One main controller in each region can be responsible for obtaining the necessary reactive support for all devices in its region. This division allows us to consider a smaller region for communication and control, since it is likely that only a subset of the controllers will need to be involved in a given response. Reactive support groups also help make this framework extensible to decentralized control algorithms where perhaps these groups could coordinate with each other instead of relying on a central control. We utilize sensitivities and several clustering approaches to form these reactive support groups.

For the RTS, some clusters formed using the VCI algorithm appear as groups in the first column of Table 6.2. For each group, we identify five supportive buses based on the maximum of the sensitivities of the voltages of the buses in column 1 to the reactive power injections at "CAT1" buses. The sensitivity to each supporter bus's reactive power injection is given beneath the bus number:

Table 6.2 Reactive Support Groups for the IEEE-24 Bus RTS

Voltage-Coupled Groups	**5 Supporter Buses and their Corresponding Sensitivities**				
4	4	9	3	8	24
	0.071	0.019	0.009	0.005	0.004
5	5	10	8	9	4
	0.050	0.012	0.003	0.002	0.001
10	10	5	8	9	4
	0.024	0.012	0.006	0.005	0.003
9,11,12	9	4	3	8	24
	0.034	0.019	0.015	0.008	0.007
15,16,17	15	24	16	19	3
	0.013	0.011	0.011	0.006	0.006
16,17,19	19	16	15	20	24
	0.017	0.011	0.006	0.006	0.005
19,20	19	20	16	15	24
	0.017	0.009	0.006	0.004	0.003
3,24	3	24	9	4	15
	0.063	0.028	0.015	0.008	0.006

The grouping in Table 6.2 uses information about how voltages can be controlled with respect to other voltages and also ensures that each voltage has at least five supporters.

This organization is flexible enough to handle problems in a decentralized way instead of always in a top-down manner, although that is not the focus of this particular work. Such a situation would not need to rely on the Central EMS to send the control messages. Thus, potential applications of the framework extend beyond voltage control and could also benefit from the use of intelligent agents.

7. Summary and Directions for Future Work

This project has presented research in six five different areas in which the measurements from PMUs can be used to enhance power system situational awareness. First, the use of Singular Value Decomposition (SVD) was presented to extract information from the PMU data without needing information about the system model. The work demonstrated that the SVD approach could be used to approximately track the maximum singular value of the inverse of the power flow Jacobian, a well established indicator for voltage instability. Still, many avenues for future work in this area remain, including practical issues such as data scaling and filtering, along with more analytic work to further determine optimal window sizes and improved heuristics.

Second, the project considered how PMU data could be used to morph a power flow case to better reflect the power system conditions associated with the PMU measurements. The application of the common LP optimal power flow approach makes this approach quite amiable for implementation in existing power system analysis packages. Based on the examples considered here the approach seems promising, but further research is needed to test the algorithm using expanded data sets and system operating conditions.

Chapter 4 presented two approaches in which information derived from Prony analysis of PMU data could be visualized to improve situational awareness associated with power system oscillations. As part of the WSU Oscillation Monitoring System (OMS), these visualizations are currently during going testing at TVA during which they will undoubtedly be further refined.

The next chapter discussed how PMU data could be used to enhance the load models used in real-time and study mode analysis software. The use of real-time measurements to enhance both static and dynamic models was considered. Based on the results presented here using simulated phasor data, the indication is that the method could become a valuable tool for model identification in real time. Additional tests need to be done on larger systems and with actual PMU data.

The last chapter looked at how PMU data could be used to improve situational awareness associated with reactive power aspects of power system operations. The research demonstrated how distributed, low voltage reactive power control devices such as solar array and PHEV inverters could be used to supply reactive power. Testing using small systems has been promising, with actual implementation in the University of Illinois campus power grid planned.

In summary, with the rapid growth in PMU installations across many power systems it is clear that PMUs will play a role of increasing importance in power system operations. This project has presented solid research in several promising areas in which this PMU information can be used to not only enhance power system situational awareness, but also to improve operations and planning in general. While the project has covered much ground, there is certainly a great need for future research.

Project Publications

Chéverez-González and C.L. DeMarco, "Mutually Orthogonal LMP Decompositions: Congestion Decomposes, Losses Do Not," to appear, 6th International Conference on the European Energy Market, Leuven, Belgium, May 27-29, 2009.

D. Cheverez-Gonzalez; C.L. DeMarco; "Admissible Locational Marginal Prices via Laplacian Structure in Network Constraints," *IEEE Transactions on Power Systems*, vol. 24, no. 1, pp. 125 - 133, Feb. 2009

K..M. Rogers, R. Klump, H. Khurana, T.J. Overbye, "Smart-Grid Enabled Load and Distributed Generation as a Reactive Resource," IEEE PES Conference on Innovative Smart Grid Technologies, Washington, DC, January 2010.

K.M. Rogers, R. Klump, H. Khurana, A. Aquino-Lugo, T.J. Overbye, "An Authenticated Control Framework for Distributed Voltage Support on the Smart Grid," *IEEE Transactions on Smart Grid*, vol. 1, June 2010, pp. 40-47.

T.J. Overbye, J.D. Weber, "The Smart Grid and PMUs: Operational Challenges and Opportunities," Proc. IEEE PES 2010 General Meeting, Minneapolis, MN, July 2010.

Shanshan Liu, "Dynamic Data-Driven Real-Time Identification for Electric Power Systems", Ph.D. dissertation, University of Illinois at Urbana-Champaign, 2009

Shanshan Liu and Peter W. Sauer, "Load Models from Measurements for Power Systems", in preparation for submission, 2010

References

[1] A.G. Phadke, J.S. Thorp, M.G. Adamiak, "A New Measurement Technique for Tracking Voltage Phasors, Local System Frequency and Rate of Change of Frequency," *IEEE Trans. on Power Apparatus and Systems*, vol. PAS-102, May 1983, pp. 1025-1038.
[2] A.G. Phadke, J.S. Thorp, K.J. Karimi, "State Estimation with Phasor Measurements," IEEE Trans. on Power Systems, vol. PWRS-1, Feb. 1986, pp. 233-238.
[3] R.E. Wilson, K.E. Martin, R. Klump, "Power System Visualization with Phasor Data," Proc. 2004 North American Power Symposium, Moscow, ID, August 2004.
[4] M. Parashar, "Real Time Dynamics Monitoring System (RTDMS), OE Visualization and Controls Peer Review, Washington, DC, October 2008.
[5] D. Kalman, "A Singularly Valuable Decomposition: The SVD of a Matrix," The College Mathematics Journal, v. 27, pp. 2-23, 1996.
[6] J. Shlens, "A Tutorial on Principal Component Analysis: Derivation, Discussion and Singular Value Decomposition," http://www.snl.salk.edu/~shlens/
[7] A. Tiranuchit, R.J. Thomas, "A Posturing Strategy Against Voltage Instabilities in Electric Power Systems," IEEE Trans. Power Sys, 1988.
[8] D.W. Allan, M.A. Weiss, "Accurate Time and Frequency Transfer During Common – View of a GPS Satellite," *Proc. 34th Ann. Freq. Control Symposium*, USAERADCOM, Ft. Monmouth, NJ, May 1980, pp. 334-346.
[9] A.G. Phadke, J.S. Thorp, M.G. Adamiak, "A New Measurement Technique for Tracking Voltage Phasors, Local System Frequency and Rate of Change of Frequency," *IEEE Trans. on Power Apparatus and Systems*, vol. PAS-102, May 1983, pp. 1025-1038.
[10] A.G. Phadke, J.S. Thorp, "History and Applications of Phasor Measurements," *Proc. IEEE Power Systems Conference and Exposition*, Oct. 29 – Nov. 1 2006, pp. 331-335.
[11] A.G. Phadke, J.S. Thorp, K.J. Karimi, "State Estimation with Phasor Measurements," *IEEE Trans. on Power Systems*, vol. PWRS-1, Feb. 1986, pp. 233-238.
[12] R. Zivanovic and C. Cairns, "Implementation of PMU Technology in State Estimation: An Overview," *Proc. IEEE AFRICON*, vol. 2, 1996, pp. 1006–1011.
[13] L. Zhao, A. Abur, "Multiarea State Estimation using Synchronized Phasor Measurements," *IEEE Trans. on Power Systems*, vol. PWRS-20, May 2005, pp. 611-617.
[14] M. Zhou, V. A. Centeno, J.S. Thorp, A.G. Phadke, "An Alternative for Including Phasor Measurements in State Estimators," *IEEE Trans. on Power Systems*, vol. PWRS-21, November 2006, pp. 1930-1937.
[15] R. Emami, A. Abur, "Robust Measurement Design by Placing Synchronized Phasor Measurements on Network Branches," *IEEE Trans. on Power Systems*, vol. PWRS-25, November 2010, pp. 38-43.
[16] A.J. Wood, B.F. Wollenberg, *Power Generation, Operation and Control*, John Wiley & Sons, New York, 1984.
[17] T.J. Overbye, X. Cheng, and Y. Sun, "A comparison of the ac and dc power flow models for LMP calculations," *Proc. 37th Hawaiian International Conference on System Sciences*, Kona, HI, January 2004.
[18] K. Purchala, L. Meeus, D. Van Dommelen, R. Belmans, "Usefulness of DC Power Flow for Active Power Flow Analysis," *Proc. IEEE PES 2005 General Meeting*, San Francisco, CA, June 2005.

[19] B. Stott, J. Hardunm, O. Alsac, “DC Power Flow Revisited,” *IEEE Trans. Power Systems*, vol. PWRS-24, August 2009, pp. 1290-1300.
[20] J. Carpienterm, “Contribution e l’étude do Dispatching Economique,” *Bulletin Society Francaise Electriciens*, Vol. 3, August 1962.
[21] H.W. Dommel, W.F. Tinney, “Optimal power flow solutions,” *IEEE Trans. Power Apparatus and Sys*tems, Oct. 1968, pp. 1866-1876.
[22] J.A. Momoh, M.E. El-Hawary, R. Adapa, “A review of selected optimal power flow literature to 1993,” *IEEE Trans. on Power Systems*, February 1999, pp. 96-111.
[23] M.E. El-Hawary et. al., *IEEE Tutorial Course, Optimal Power Flow: Solution Techniques, Requirements and Challenges*, IEEE 96 TP 110-0, 1996.
[24] B. Stott and J.L. Marinho, “Linear programming for power system network security applications,” *IEEE Trans. on Power Apparatus and Systems*, Vol. PAS-98, May/June 1979, pp. 837-848.
[25] G.B. Dantzig, M.N. Thapa, *Linear Programming*, Springer, New York, NY, 1997.
[26] T. J. Overbye, "Estimating the actual cost of transmission system congestion," *Proc. 36th Hawaii International Conference on System Sciences*, Kona, HI, January 2003.
[27] O. Alsac, J. Bright, M. Prais, B. Stott, “Further developments in LP-based optimal power flow,” *IEEE Trans. on Power Systems*, August 1990, pp. 697-711.
[28] G. Liu, J. Quintero, and V. Venkatasubramanian, “Oscillation Monitoring System based on wide area synchrophasors in power systems,” *Proc. IREP symposium 2007*. Bulk Power System Dynamics and Control - VII, August 19-24, 2007, Charleston, South Carolina, USA.
[29]] G. Liu and V. Venkatasubramanian, "Oscillation monitoring from ambient PMU measurements by Frequency Domain Decomposition," *Proc. IEEE International Symposium on Circuits and Systems*, Seattle, WA, May 2008, pp. 2821-2824.
[30] G. Liu, V. Venkatasubramanian, and J. R. Carroll, “Oscillation Monitoring System using Synchrophasors”, Proc. IEEE General Power Meeting, Calgary, CA, July 2009.
[31] V. Venkatasubramanian and J. R. Carroll, “Oscillation Monitoring System at TVA”, presentation at NASPI meeting, New Orleans, LA, Mar. 2008, at http://www.naspi.org/meetings/workgroup/2008_march/session_one/tva_oscillation_monitoring_venkatasubramanian.pdf
[32] C. W. Taylor, *Power System Voltage Stability*. New York, NY: McGraw-Hill, 1994.
[33] IEEE Task Force on Load Representation for Dynamic Performance, "Load representation for dynamic performance analysis," *IEEE Transactions on Power Systems*, vol. 8, no. 2, pp. 472-482, May 1993.
[34] D. J. Hill, "Nonlinear dynamic load models with recovery for voltage stability studies," *IEEE Transactions on Power Systems*, vol. 8, no. 1, pp. 166-176, Feb. 1993.
[35] W. W. Price et al., "Load modeling for power flow and transient stability computer studies," *IEEE Transactions on Power Systems*, vol. 3, no. 1, pp. 180-187, Feb. 1988.
[36] W. Xu and Y. Mansour, "Voltage stability analysis using generic dynamic load models," *IEEE Transactions on Power Systems*, vol. 9, no. 1, pp. 479-493, May 1994.
[37] U.S.-Canada Power System Outage Task Force, "Final report on the August 14, 2003 blackout in the United States and Canada," April 2004.
[38] C. W. Taylor, *Power System Voltage Stability*. New York, NY: McGraw-Hill, 1994.

[39] IEEE Task Force on Load Representation for Dynamic Performance, "Load representation for dynamic performance analysis," *IEEE Trans. on Power Systems*, vol. 8, no. 2, pp. 472-482, May 1993.
[40] C.-J. Lin et al., "Dynamic load models in power systems using the measurement approach," *IEEE Trans. on Power Systems*, vol. 8, no. 1, pp. 309-315, Feb. 1993.
[41] CIGRE Task Force 38-02-10, "Modeling of voltage collapse including dynamic phenomena," CIGRE Brochure No. 75, 1993.
[42] M. A. Merkel and A. M. Miri, "Modelling of industrial loads for voltage stability studies in power systems," in *Canadian Conference on Electrical and Computer Engineering, 2001*, May 2001, pp. 0881-0886.
[43] PSS/E, *Power system simulator for engineering*. Schenectady, NY: Siemens - Power Technologies Inc.
[44] Chow and G. Rogers, "Power Systems Toolbox." [Online]. Available: http://www.eagle.ca/~cherry/pst.htm.
[45] K. M. Rogers, R. Klump, H. Khurana, A. Aquino-Lugo, T. J. Overbye, "An Authenticated Control Framework for Distributed Voltage Support on the Smart Grid," *IEEE Transactions on Smart Grid*, 2010
[46] K. M. Rogers, R. Klump, H. Khurana, T. J. Overbye, "Smart-Grid-Enabled Load and Distributed Generation as a Reactive Resource," *Proceedings of the 2010 IEEE PES Conference on Innovative Smart Grid Technologies*, Jan. 2010.